DESIGN GUIDELINES FOR INVERTER FED MOTOR DRIVES IN DISTRIBUTED POWER SYSTEM APPLICATIONS
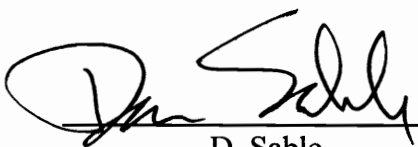
by

Musiri S.P. Shrivathsan

Thesis submitted to the Faculty of the

Virginia Polytechnic Institute and State University

in partial fulfillment of the requirements for the degree of

Master of Science

in

Electrical Engineering

APPROVED:

F.C. Lee

F.C. Lee, Chairman

Borojevic   *D. Sable*

D. Borojevic   D. Sable

July 1995

Blacksburg, Virginia

DESIGN GUIDELINES FOR INVERTER FED MOTOR DRIVES IN DISTRIBUTED POWER SYSTEM APPLICATIONS

by

Musiri S.P. Shrivathsan

Fred C. Lee, Chairman

Electrical Engineering

(ABSTRACT)

A distributed power system (DPS) is made up of several subsystems. For example, a two-stage distributed power system is made of a source subsystem consisting of line conditioners and a load subsystem consisting of loads. Motor drives used as a load subsystem form an important type of load in distributed power system applications. The input impedance of the load subsystem is an important factor in designing and analyzing the performance and stability of a distributed power system. In this thesis, a typical three-phase inverter-fed ac motor drive is modeled, analyzed and the input impedance characteristics are studied for the first time. Motor drives are found to have unique input impedance characteristics due to their electromechanical nature. The influence of these characteristics on the distributed power system are analyzed. The unique interaction problems that these characteristics lead to are studied. It is shown that a distributed power system designed without taking into account the unique input impedance characteristics of motors might suffer from performance degradation or might even become unstable. Design guidelines to avoid this situation in a distributed power system that uses motor drives as a load subsystem are developed and presented.

ACKNOWLEDGMENTS

I would like to express my sincere gratitude to my advisor, Dr. Fred C. Lee for his guidance, support, encouragement, and patience which allowed me to complete this work. I would also like to thank him for providing me with the opportunity to work at the Virginia Power Electronics Center (VPEC).

I am grateful to Dr. Dusan Borojevic, and Dr. Dan Sable for serving on my committee and their suggestions during the course of this work. I am also grateful to Dr. Bo Cho for his guidance during the course of my stay at VPEC.

I would like to thank my fellow graduate students at VPEC who have helped with both technical discussions and social interactions: all made my time at VPEC enjoyable and rewarding. My special thanks go to Carlos Cuadros, Sundar Sankaran, and Yuri Panov.

I would like to thank all my friends for all they have done for me.

Finally I would like to express my deepest appreciation to my parents, sister and my late grandmother. Their love was a never ending impetus throughout my academic career.

TABLE OF CONTENTS

CHAPTER 1

INTRODUCTION

With the rapid advances in electronic power processing technology, there have been increasing demands placed on power supply systems. Stringent requirements are placed upon system power density, transient response, efficiency and speed.

The centralized power system which uses a single regulator is often not sufficient to meet these requirements. In a power system with a single centralized power supply, the power must be distributed to the load at a low voltage level required for the load. This leads to high current levels and subsequently, high conduction losses. In addition, it is difficult to tightly regulate the load voltage level, which is necessary for sensitive loads.

To meet the demanding requirements of today's power processing systems, the distributed power system (DPS) is becoming the power system of choice. A

DPS consists of multiple cascaded power supplies; the schematic of a typical two-stage DPS is shown in Figure 1.1. The line conditioners take the unregulated dc input voltage and regulate it to an intermediate voltage bus. This bus voltage is then distributed through the system to load converters, which convert the bus voltage to a tightly regulated load voltage level needed for the loads. With the distributed power system, high power density and high efficiency can be achieved; conduction losses can be decreased; and load converters can be directly mounted at the point of load to provide tighter load voltage regulation [1].

The multi-stage distributed architecture offers many advantages over the single-stage centralized system, but the price paid for using a DPS is an increase in system complexity. Due to the size and complexity of complete DPS, it is not feasible to design such a power system as a whole. The system is typically defined in terms of several smaller subsystems, and each subsystem is designed individually. The subsystems are then integrated to form a complete DPS. Figure 1.1 shows a typical two-stage DPS consisting of a source subsystem and a load subsystem.

One of the most important issues when integrating the subsystems to build the DPS is the possible stability problems and performance degradations resulting from the interactions between the subsystems. Even though the subsystems may be well designed for stand-alone operation, this interaction can lead to stability and performance problems after system integration [1,3,4,5].
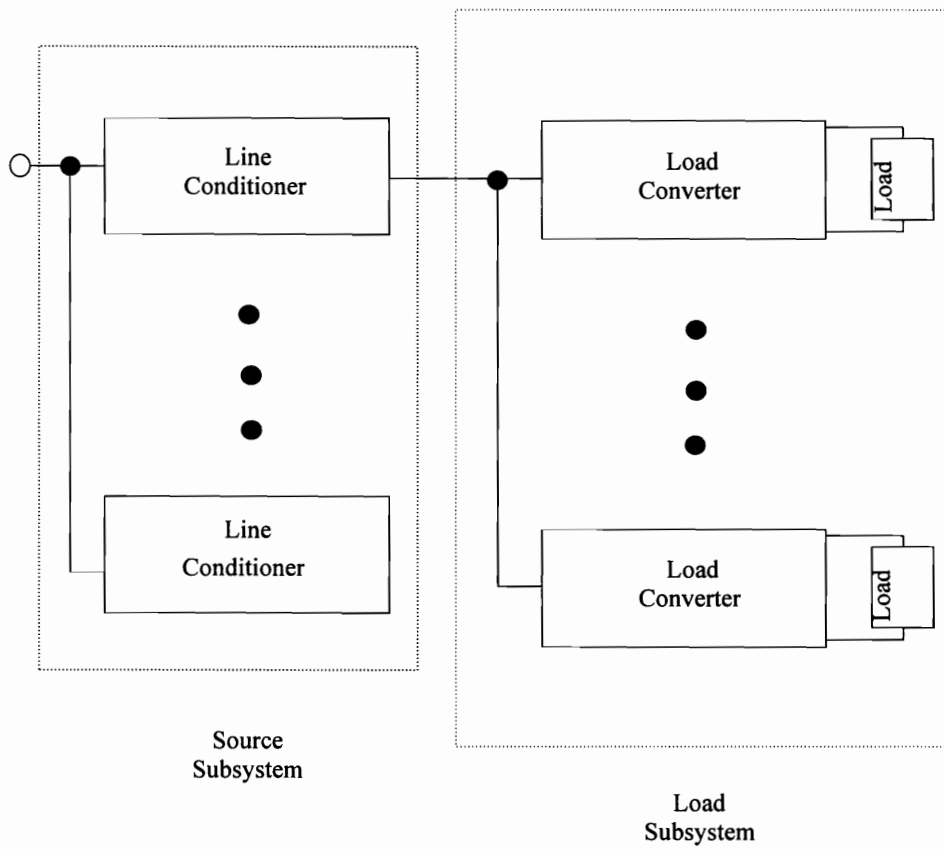
Figure 1.1 Block Schematic of a Typical Two-stage Distributed Power System

Impedance comparison techniques have been widely used for analyzing the stability issues arising from the interconnection of subsystems in a distributed power system [1,3,4,5]. Impedance comparison technique is considered the principal technique for designing and analyzing distributed power systems. This technique uses the concept of linearizing the system around the steady-state operating point and the resulting small-signal model. The output impedance of the source subsystem (Z_{OS}) and the input impedance of the load subsystem (Z_{IL}) are determined and compared to analyze the interaction between the two subsystems. The main advantage of using the impedance comparison technique lies in its simplicity and is well established [1,3,4,5]. A comprehensive stability analysis of a distributed power system is performed based on impedance comparison technique in [5]. A method of forming load impedance specifications to ensure small signal stability of the DPS is also given in [5] based on impedance comparison techniques.

Most of the common loads that form the load subsystem of a distributed power system including power supply loads (constant power loads), heater loads (resistive loads), and constant current loads have been modeled and their input impedance (Z_{IL}) characteristics have been determined [1,3,6,7]. Using these, the influence of these loads on the source subsystem of a distributed power system have been analyzed [1,3,5,6,7] in the past.

Motor drives are another important type of load that can constitute the load subsystem in a distributed power system. Typical applications of motor drives include pumps and compressors, servo, fans, blowers, conveyors, electrical traction, etc. An example of a distributed power system having motor drives as loads is the Space Station power system shown in Figure 1.2. Another example is the hybrid electric vehicle power distribution system shown in Figure 1.3.

However, motor drives constituting a load subsystem have seldom been modeled and analyzed to determine their input impedance (Z_{IL}) in the past; neither has their influence on the source subsystem of a distributed power system been studied.

This thesis models and analyzes the input impedance characteristics of a typical inverter-fed ac motor drive using a three-phase permanent magnet synchronous motors (PMSM) and a three-phase voltage source inverter (VSI) as representative circuits. The input impedance characteristics of the motor drive are compared to those of the other aforementioned loads, and are found to be unique in nature. The various interaction problems that these unique characteristics leads to are studied and illustrated. Design guidelines to avoid these interaction problems in distributed power systems employing motor drives as a part of their load subsystem are developed and presented in this thesis.

General stability issues arising while integrating subsystems in a DPS are discussed in Chapter 2. A two-stage DPS is used to demonstrate that overlap
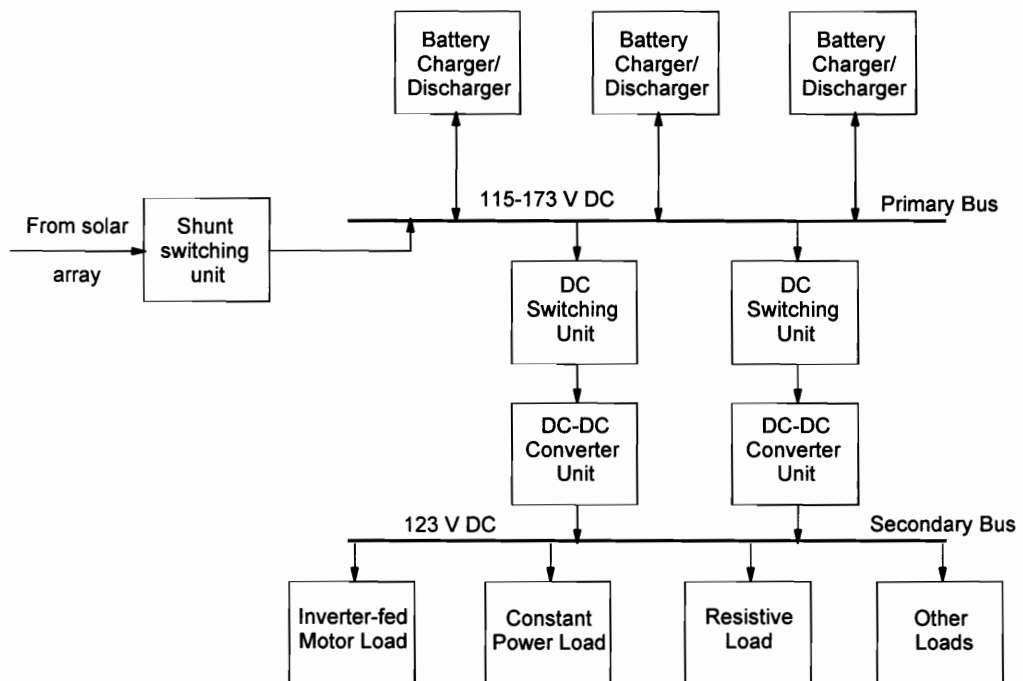
**Figure 1.2 Simplified Block Schematic of Space Station Power System
Showing Inverter-fed Motor Loads**
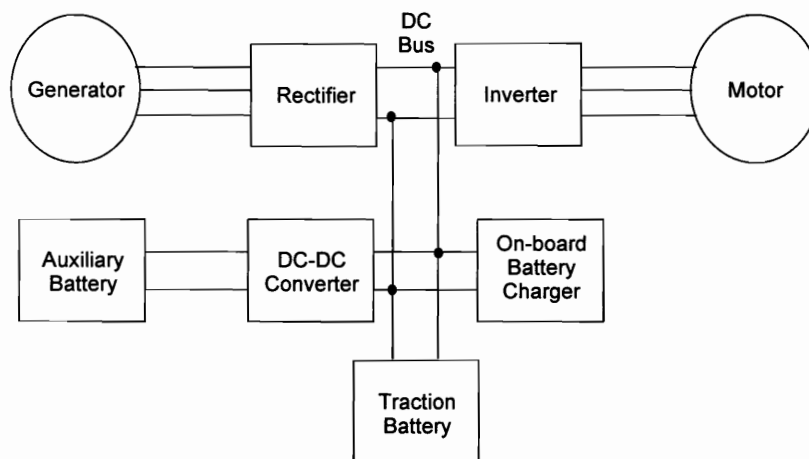
**Figure 1.3 Simplified Schematic of a Hybrid Electric Vehicle
Power System Showing Inverter-fed Motor**

between the output impedance of the source subsystem (Z_{OS}) and the input impedance of the load subsystem (Z_{IL}) can lead to performance degradation and even large-signal instability. It is shown that the input impedance of a load subsystem (Z_{IL}) along with the output impedance of the source subsystem (Z_{OS}) is an important factor in designing and analyzing the DPS.

Chapter 3 presents the modeling of three-phase permanent magnet synchronous motor (PMSM) which is used as an example of a typical three-phase motor. The model of three-phase voltage source inverter (VSI) that is used to drive the motor is also presented. The models are represented in equivalent electrical circuit form that facilitates analysis. The motor and inverter are modeled using the d-q axis transformation technique [8, 9, 10]. This is done in order to get time-invariant small-signal models of the motor and inverter. Using these models, the input impedance characteristics of the inverter-fed motor drive mentioned above are analyzed in two operating modes. The input impedances are compared to that of the other aforementioned loads namely constant power, resistive and constant current loads. The differences arising from the electromechanical nature of the motor are highlighted.

The influence of the unique input impedance characteristics of the motor drive on the distributed power system is analyzed in Chapter 4. The various interaction problems that this unique input impedance characteristics lead to are studied and illustrated using a series of examples. From these examples, it is shown that a

distributed power system design procedure that does not take into account the unique input impedance characteristics of the motor drive can lead to performance degradation or even instability of the DPS. Design guidelines to avoid the interaction problems due to these unique input impedance characteristics, while designing motor drives for use as load subsystem in a DPS are developed and presented.

Chapter 5 presents the conclusions of this thesis.

CHAPTER 2

STABILITY ISSUES IN DISTRIBUTED POWER SYSTEMS

2.1 Introduction

When designing and analyzing a distributed power system (DPS), it is often impractical to analyze the DPS as a whole to determine system stability because of the complexity of the system. The DPS is usually broken into smaller subsystems to make the design and analysis more feasible. After designing and analyzing the individual subsystems, the subsystems are then interconnected to form the DPS. One of the major difficulties in DPS analysis involves the problems arising due to interaction between the subsystems. Even for well designed subsystems, potential interaction problems may arise when the subsystems are interconnected to form the DPS.

This chapter discusses the issue of interaction between subsystems, and its effect on the DPS. Through this discussion it is shown that the input impedance of the load subsystem is a major factor that influences the interaction between the source and load subsystems, which may lead to performance degradation of the DPS or even instability.

2.2 Interconnection of two subsystems

Figure 2.1 shows two subsystems namely, source subsystem and load subsystem interconnected to form an integrated system. It is assumed that the two subsystems are stable and well-designed for stand-alone operation. F_S is the transfer function of the source subsystem and F_L is the transfer function of the load subsystem. It can be found that the integrated system transfer function is [1]:

$$F_{SL} = \frac{V_O}{V_{IN}} = \frac{F_S * F_L}{(1 + T_M)}$$

(2.1)

where:

$$T_M = \frac{Z_{OS}}{Z_{IN}},$$

(2.2)

Source
Subsystem

Load
Subsystem

V_1

$+$

V_{IN}

$F_S = V_1/V_{IN}$

$+$

$-$

$F_L = V_O/V_1$

$+$

V_O

$-$

Z_{OS} Z_{IL}

Integrated
System
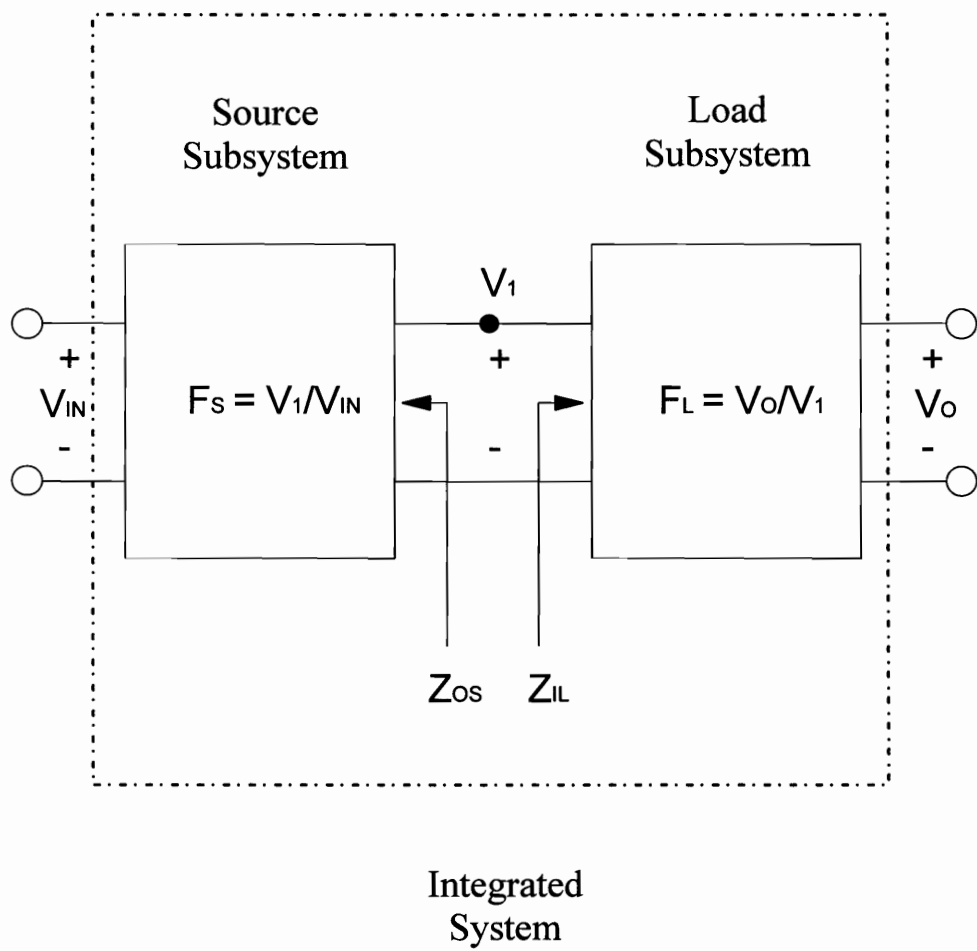
$$F_{SL} = V_O/V_{IN} = F_S{\cdot}F_L/(1+(Z_{OS}/Z_{IL}))$$

Figure 2.1 Two interconnected subsystems

F_S = Forward voltage gain of Source subsystem without load,

F_L = Forward voltage gain of Load subsystem without source,

Z_{OS} = Output impedance of the Source subsystem, and

Z_{IL} = Input impedance of the Load subsystem.

It can be seen that the term $(1+T_M)$ represents the loading effect caused by integrating the subsystems. Both F_S and Z_{OS} have common denominators, as do F_L and $1/Z_{IL}$; this is because both these pairs are input-output transfer functions which have the same characteristic equation. Using this, and assuming all eigenvalues of each subsystem are observable at the output port, the characteristic equation for the overall system can be derived as [1]:

$$1+T_M = 0.$$

(2.3)

Based upon this derivation of the characteristic equation, the term T_M, due to the loading effect can be viewed as a system equivalent loop gain. This system loop gain can be used to determine the integrated system performance. The integrated system stability can be determined by applying the Nyquist criteria to this loop gain [1,5].
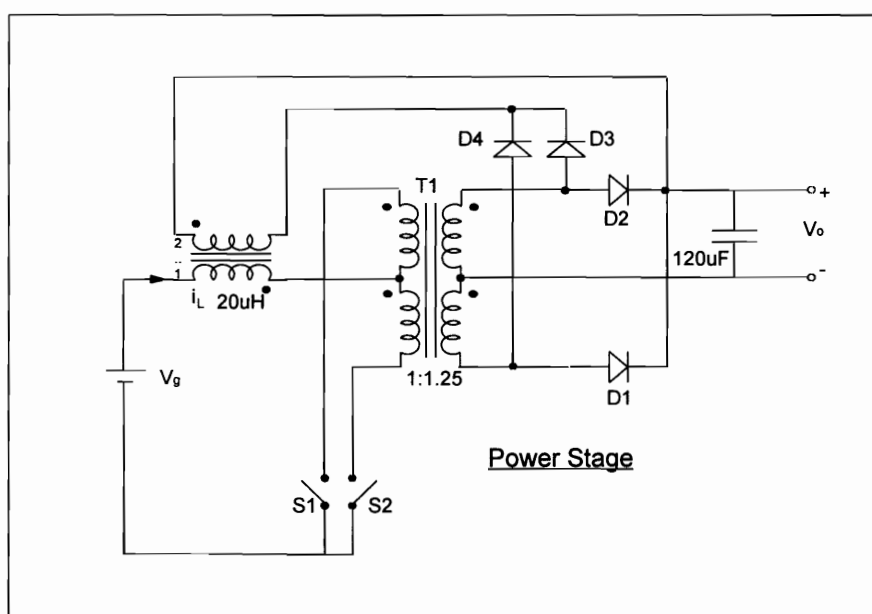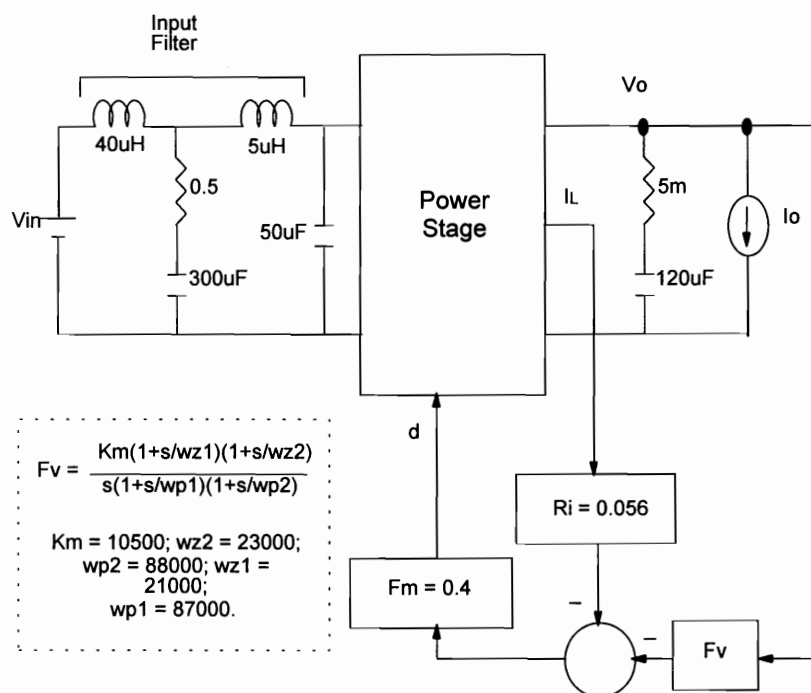
2.3 Example System

Through out the remainder of this chapter, a two-stage DPS is used as an example. The source subsystem consists of a dc-dc converter unit (DDCU) designed for use in Space Station. Load converters with their input filters will be used to form the load subsystem.

A circuit diagram of the source subsystem is shown in Figure 2.2. The DDCU power stage is a pulse width modulated (PWM) current fed buck-derived converter (Weinberg converter) [5] which regulates an input voltage between 115 V - 173 V to a 123 V bus. The DDCU can supply loads in the range of 70 W - 6.5 kW. This source subsystem (DDCU) is modeled by state-space averaging approach. The resulting large-signal model is perturbed and linearized to get the small-signal model of the source subsystem [5].

The input filter of the load converters with a negative resistance load is used to simulate the load subsystem. This approximation is valid to simulate the input impedance of load converters [3,6,7].

2.4 Effect of overlap between Z_{OS} and Z_{IL} on Integrated system stability

It can be seen from equations (2.2) and (2.3) that $[Z_{OS} / Z_{IL}]$ $(=T_M)$ is a loop gain and therefore can be used to analyze the integrated system stability and

$$Fv = \frac{Km(1+s/wz1)(1+s/wz2)}{s(1+s/wp1)(1+s/wp2)}$$

Km = 10500; wz2 = 23000;
wp2 = 88000; wz1 = 21000;
wp1 = 87000.

**Figure 2.2 Circuit Diagram of DC-DC Converter used as Source Subsystem**

performance. From equation (2.1), it can be observed that if $|Z_{IL}| >> |Z_{OS}|$ at all frequencies, then $T_M << 1$ and hence the denominator of equation (2.1) is approximately unity. This means there is minimal interaction between the subsystems. In such a case, the integrated system performance will depend primarily upon the performance of the two individual subsystems only. However, if there is an overlap between $|Z_{OS}|$ and $|Z_{IL}|$, then at some frequencies, $|T_M| \geq 1$. And if at these frequencies, the difference between the phases of Z_{OS} and Z_{IL} is 180 degrees, then the Nyquist plot of T_M, goes through or encircles (-1,0) point and this leads to instability in the integrated system [1,5]. If, the difference between the phases of Z_{OS} and Z_{IL} is less than but close to 180 degrees, then the integrated system will have a small phase margin, and is susceptible to become unstable upon large-signal disturbance [1,5]. Thus the input impedance of the load subsystem (Z_{IL}) and the output impedance of the source subsystem (Z_{OS}) are important factors that determine the level of interaction between the two subsystems when they are interconnected to form the integrated system [1,5].
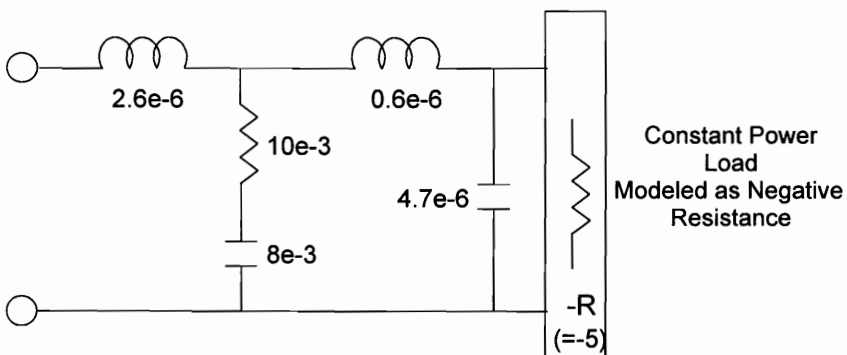
2.5 Study of Example System

In this section the example system defined in Section 2.3 will be studied with the DDCU as the source subsystem and three different load subsystems. The three example load subsystems are shown in Figure 2.3.
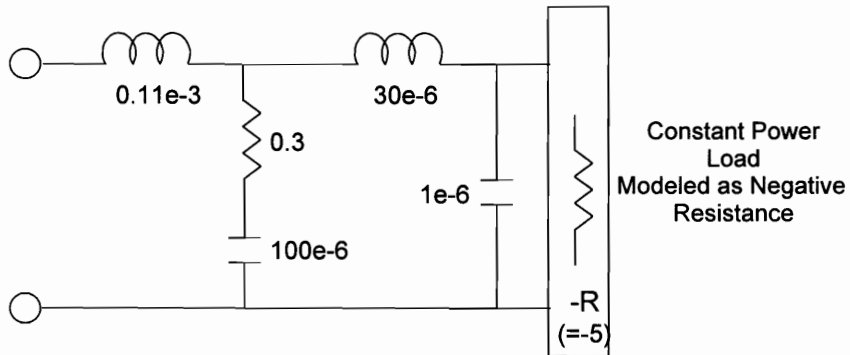
Example Load subsystem 1
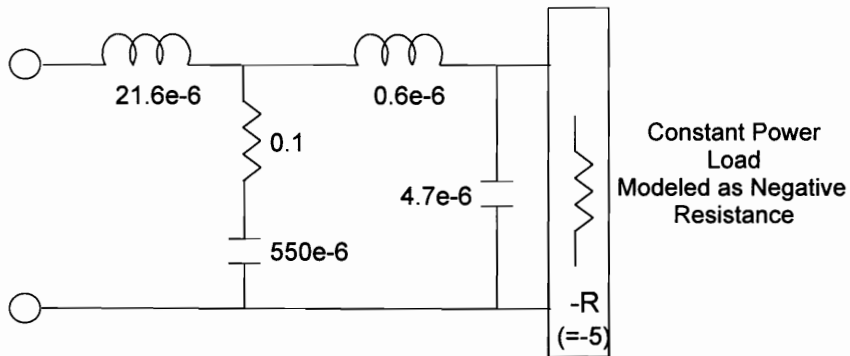
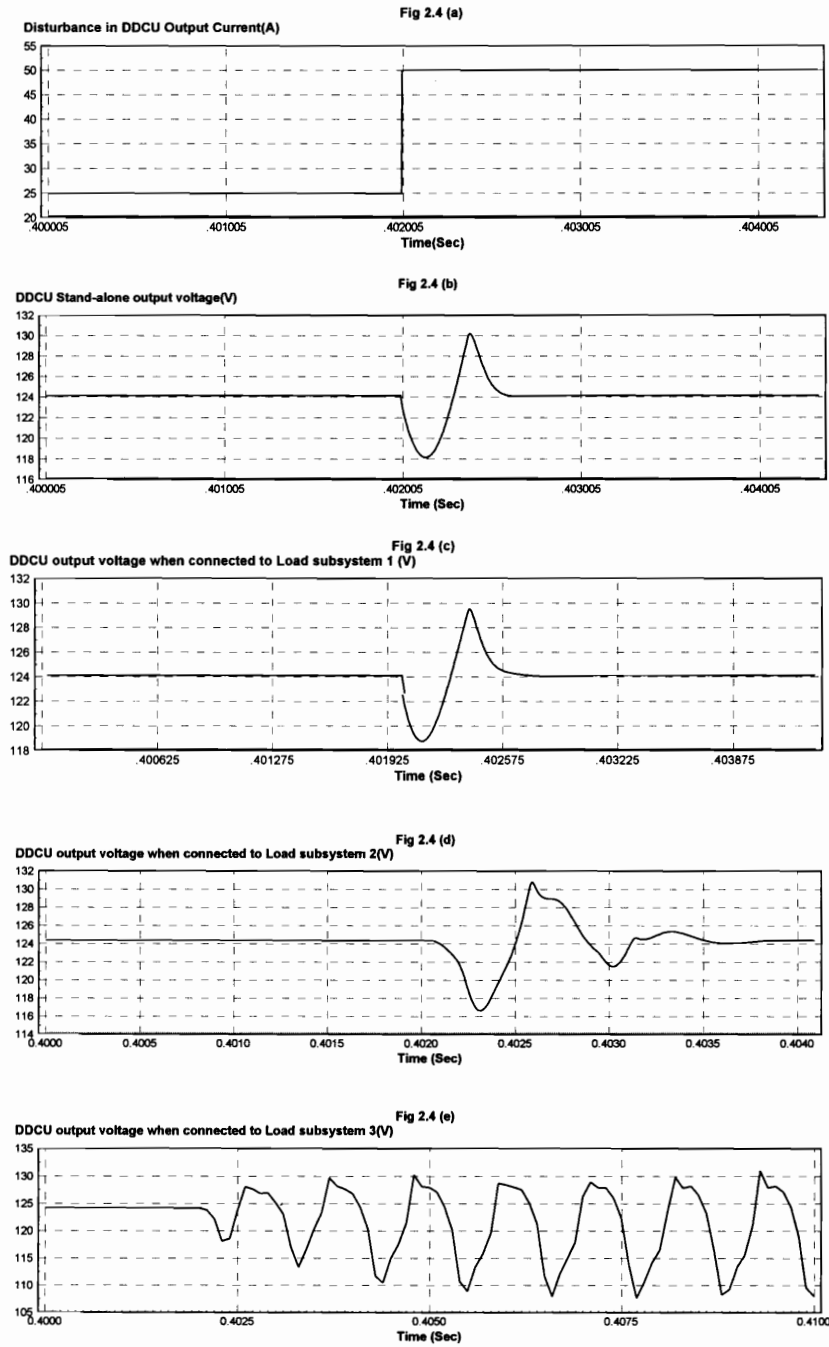**Example Load subsystem 2**

Example Load subsystem 3

Figure 2.3 Example Load subsystems

First, in order to study the dynamics of the source subsystem in stand-alone operation, a disturbance in the output current of the source subsystem is applied from a steady state of 25 A to 50A. This disturbance is shown in Figure 2.4 (a). The resultant output voltage of the source subsystem is shown in Figure 2.4 (b). This shows the dynamics of the source subsystem in its stand-alone operation.

Figure 2.5 shows the output impedance of the source subsystem compared with the input impedances of the three example load subsystems of Figure 2.3. It can be seen that in the case of Load subsystem 1, $|Z_{IL1}| \gg |Z_{OS}|$ at all frequencies. The resultant output voltage of the source subsystem when the above-mentioned disturbance is applied to the integrated system formed by interconnecting the Source subsystem and Load subsystem 1 is shown in Figure 2.4 (c). It can be seen that the dynamics of this integrated system is determined by that of the individual subsystems only and there is no significant performance degradation due to the interconnection of the two subsystems.

Now another integrated system is formed by interconnecting the Source subsystem and Load subsystem 2. From Figure 2.5, it can be seen that there is an overlap between $|Z_{OS}|$ and $|Z_{IL2}|$. The resultant output voltage of the Source subsystem when the example disturbance is applied to this integrated system is shown in Figure 2.4 (d). It is seen that the waveform is oscillatory and the settling time is more compared to the previous two cases. This clearly shows that the

Fig 2.4 (a)
Disturbance in DDCU Output Current(A)

Fig 2.4 (b)
DDCU Stand-alone output voltage(V)

Fig 2.4 (c)
DDCU output voltage when connected to Load subsystem 1 (V)

Fig 2.4 (d)
DDCU output voltage when connected to Load subsystem 2(V)

Fig 2.4 (e)
DDCU output voltage when connected to Load subsystem 3(V)

Figure 2.4 Transient Response of Source Subsystem In stand-alone mode (b) and when connected to Load Subsystems of Figure 2.3 (c,d,e)

18
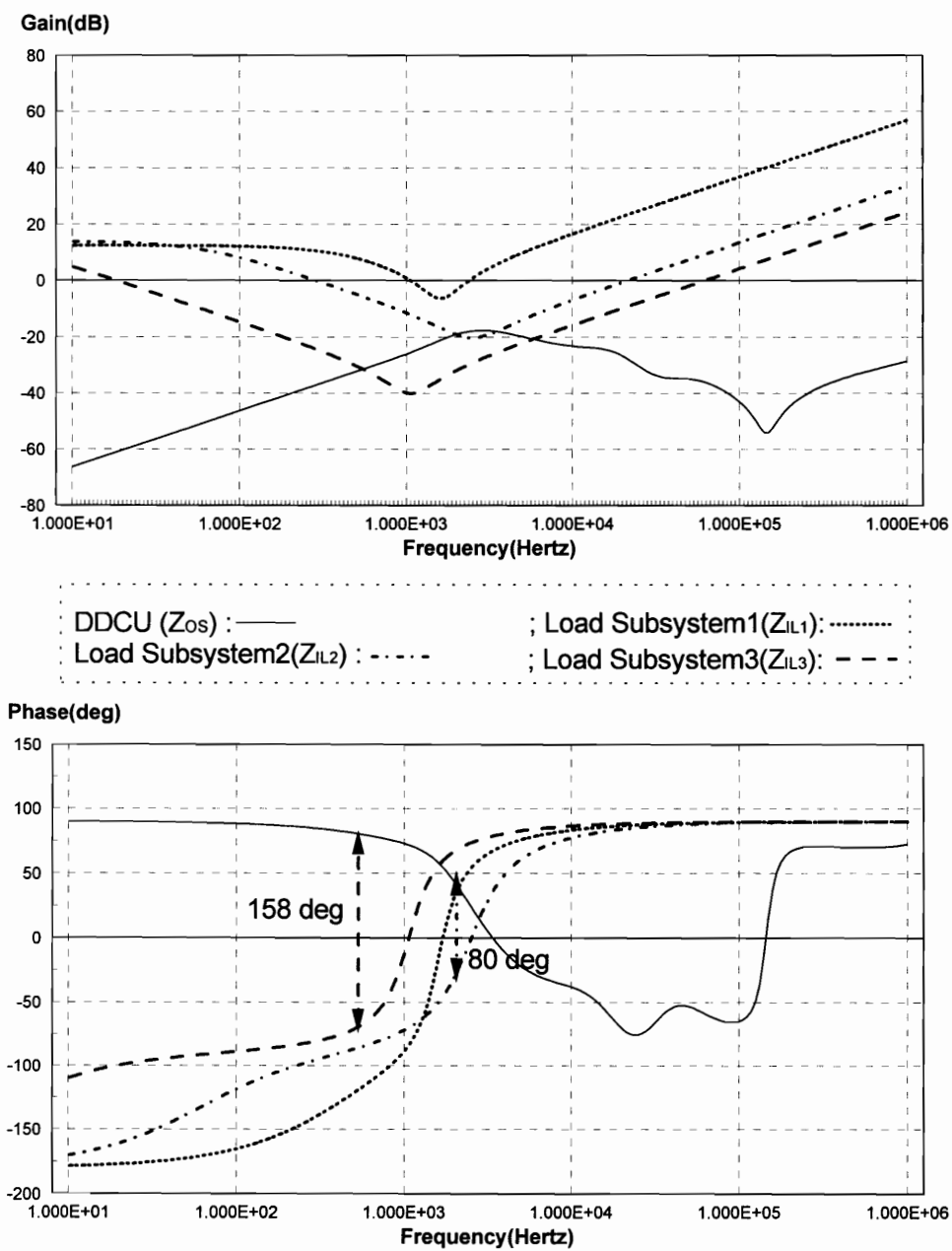
Figure 2.5 Comparison of Output Impedance of Source subsystem (Z$_o$) and Input Impedances (Z$_{in}$) of three Load subsystems

overlap between $|Z_{OS}|$ and $|Z_{IL2}|$ leads to performance degradation of the integrated system. It is also seen from Figure 2.5 that the difference in the phases of Z_{OS} and Z_{IL} at the cross-over frequency of T_M is 80 degrees. Hence, the integrated system has sufficient phase margin. As a result, even though there is performance degradation, the integrated system is still stable.

Now, an integrated system is formed by interconnecting the Source subsystem and Load subsystem 3. From Figure 2.5, it can be seen that there is a significant overlap between $|Z_{OS}|$ and $|Z_{IL2}|$. The resultant output voltage of the Source subsystem when the example disturbance is applied to this integrated system is shown in Figure 2.4 (e). It is seen that there is sustained oscillation in the output voltage and instability has crept in. It can be seen from Figure 2.5 that the difference in the phases of Z_{OS} and Z_{IL} at the crossover frequency of T_M is 158 degrees. Hence, the integrated system has a small phase margin (22 degrees) even though it is small signal stable. When the large signal disturbance is applied to this system, it excites the nonlinearity in the system namely the duty cycle saturation. As a result of the large signal disturbance the system goes into sustained large-signal oscillations and thus becomes large signal unstable. [11] has a more detailed discussion on large signal stability of the integrated distributed power system.

From the foregoing discussion it can be summarized that, when integrating two subsystems, namely a source subsystem with an output impedance of Z_{OS} and

a load subsystem with an input impedance of Z_{IL} to form an integrated subsystem, in order to ensure minimal interaction between the subsystems the following criterion should be met [5]:

Criteria:

There should be no overlap between $/Z_{OS}/$ and $/Z_{IL}/$,

or

When there is an overlap between $/Z_{OS}/$ and $/Z_{IL}/$, the difference between $\angle Z_{OS}$ and $\angle Z_{IL}$ in the range of frequencies where there is an overlap between $/Z_{OS}/$ and $/Z_{IL}/$ should be less than 180 degrees [5].

(Criterion 2.1)

Also in order to ensure large signal stability in the integrated system in the presence of nonlinearities like duty cycle saturation it should be ensured that T_M has a sufficient phase margin.

2.6 Summary

The interaction problems that arise while integrating the subsystems of a DPS were illustrated using a two-stage DPS as an example. Using three examples it was shown that the input impedance of the load subsystem is an important design and analysis parameter in a DPS. From these examples, it was shown that when two subsystems that are stable and have good performance in stand-alone

operation are interconnected to form an integrated system, performance degradation or even instability might result in the integrated system. It was shown that when designing a DPS by interconnecting subsystems, the impedances of individual subsystems should be compared and overlap between them if any should be analyzed in order to determine the level of interaction between the subsystems, and the performance of the DPS.

CHAPTER 3

MODELING AND STUDY OF INPUT IMPEDANCE

CHARACTERISTICS OF INVERTER FED MOTOR DRIVES

3.1 Introduction

One common design approach for the two-stage DPS is to design the source subsystem separately using an ac unterminated modeling approach [12]. Once the source subsystem is designed, the output impedance of the source subsystem (Z_{OS}) is known. Then the load subsystem can be designed such that there is minimal interaction between the input impedance of the load subsystem (Z_{IL}) and Z_{OS}. To follow this procedure, it is imperative to know the input impedance characteristics of the load subsystem. Load subsystems can be formed by different types of loads like power converter loads, heater loads, current sink loads. These

loads have been modeled and analyzed to understand their input impedance characteristics [1,3,5,6,7,11,12]. Motor drives used to convert the electrical energy output of the source subsystem into some useful form of mechanical energy form another important kind of loads. But modeling and analysis of input characteristics of motor drives used as load subsystem of a DPS have seldom been performed in previous literature [1,3,5,6,7,11,12].

In order to study the issues arising while designing an inverter fed motor drive for use as the load subsystem of a DPS, a typical inverter fed motor drive system shown in Figure 3.1 will be used as an example system throughout this thesis, unless mentioned otherwise.

As can be seen from Figure 3.1 this drive system consists of three blocks: the motor, the inverter and the EMI filter used to attenuate the switching frequency (of the inverter) ripple in the input current of this drive system. In this thesis a permanent magnet synchronous motor (PMSM) will be studied as a typical example of three-phase motors.

A most commonly used type of inverter namely, voltage source inverter (VSI) will be used as the inverter used to drive the motors. A very popular two-stage LC filter topology shown in Figure 3.2 will be used as the front-end EMI filter of the inverter-fed motor drive system.

Since the motor and inverter to be studied are three-phase circuits, d-q co-ordinate transformation technique [8] will be used to derive the models of motor
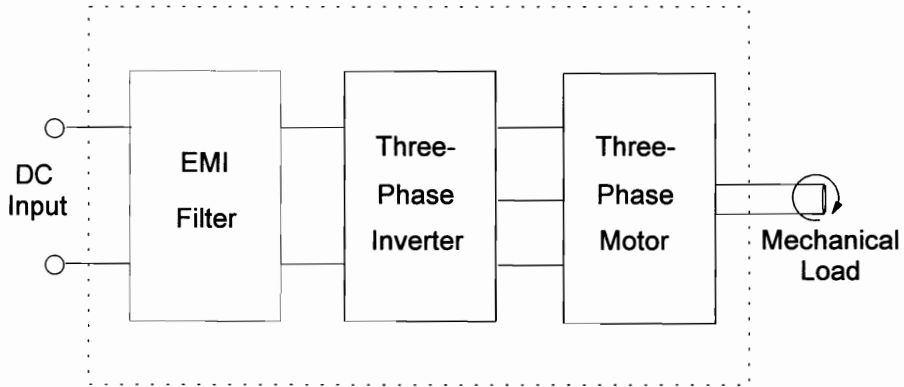
Figure 3.1 A typical inverter fed motor drive system
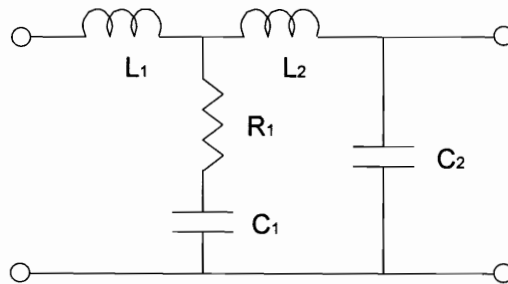
Figure 3.2 A typical two-stage LC (EMI) filter topology

and inverter; this helps in getting time-invariant small-signal models of the motor and the inverter [9,10].

Using these models, the input impedance characteristics of the drive system shown in Figure 3.1 will be studied for the motor. Two operating modes of the motor will be studied and input impedances for both modes will be analyzed. The first mode is operation with speed regulation which is used for applications like constant speed drives, conveyors etc. The second mode of operation is operation without speed regulation which is used in applications like fans, blowers, etc.

3.2 Modeling of the Inverter-Fed Motor Drive System

3.2.1 Modeling of Three-Phase Permanent Magnet Synchronous Motor (PMSM)

Three-phase permanent magnet synchronous motor (PMSM) is a synchronous motor with its field coil, dc power supply, and slip rings replaced by a permanent magnet [8,9]. It has been shown [13] that PMSM has a higher-torque-to-inertia ratio and higher power density when compared to the induction motor or wound rotor synchronous motor, which makes it preferable for high-performance applications like aerospace actuators, robotics, etc.

The rotor of the PMSM has permanent magnets made of modern rare-earth materials [9,13] and hence induced currents in the rotor are negligible. With this

fact and the assumptions listed below, equations (3.1) - (3.5) represent the model of the PMSM [8,9].

Assumptions made in deriving the model:

i) Saturation is neglected.

ii) Induced EMF is sinusoidal.

iii) Eddy currents and hysterisis losses are negligible.

iv) There are no field dynamics.

The stator voltage equations in d-q co-ordinates (in rotor reference frame) are given by [8,9]:

$$v_d = R\ i_d + L\ \frac{di_d}{dt} - w_s\ L\ i_q$$

(3.1)

$$v_q = R\ i_q + L_q\ \frac{di_q}{dt} + w_s\ (L\ i_d + \psi)$$

(3.2)

Torque produced is given by [8,9]:

$$m_p = \frac{3}{2}\ P\ \psi\ i_q$$

(3.3)

The equation for motor dynamics is [8,9]:

$$m_p = m_L + D\ w_r + J\ \frac{dw_r}{dt}$$

(3.4)

In these equations:

v_d, v_q - d, q axis stator voltages (V) of PMSM respectively.

i_d, i_q - d, q axis stator currents (A) of PMSM respectively.

L, R - Stator inductance (H) and stator resistance (Ω) of PMSM respectively.

ψ - Stator-to-rotor mutual linkage V/rad/sec.

w_s - inverter output frequency (rad/sec).

w_r - Speed of rotor (rad/sec).

P - Number of pair of poles of PMSM.

J - Moment of inertia (kg-m^2).

D - Damping co-efficient (n-m/rad/sec).

m_p - Torque produced by the motor (N-m).

m_L - Load torque (N-m).

In these equations w_r and w_s are related by:

$$w_s = P\ w_r$$

(3.5)

Equations (3.1) - (3.5) are represent the large signal model of PMSM and can be represented in equivalent electric circuit form as shown in Figure 3.3. The equivalent electric circuit consists of three interdependent subcircuits. The two subcircuits on the left in Figure 3.3 represent the q and d-axis electrical part of the PMSM. The subcircuit on the right represents the electromechanical part of the PMSM. The torques are represented in this equivalent model as current sources, while back emf is represented as a voltage source of value $w_s^* \psi$. Moment of inertia (J) appears as a capacitor in this model, while mechanical damping (D) appears as a conductance. Other parts of this model are self-explanatory.

The inputs and the state variables of this model are perturbed as given by the following equations:

$$i_q = I_q + i_q^p$$

$$i_d = I_d + i_d^p$$

$$w_r = \Omega_r + w_r^p$$

$$v_q = V_q + v_q^p$$

$$v_d = V_d + v_d^p$$

$$m_L = M_L + m_L^p$$

$$(3.6)$$

In equations (3.6), uppercase alphabets represent the steady-state values of the variables and superscript 'p' is used to represent small-signal perturbation in
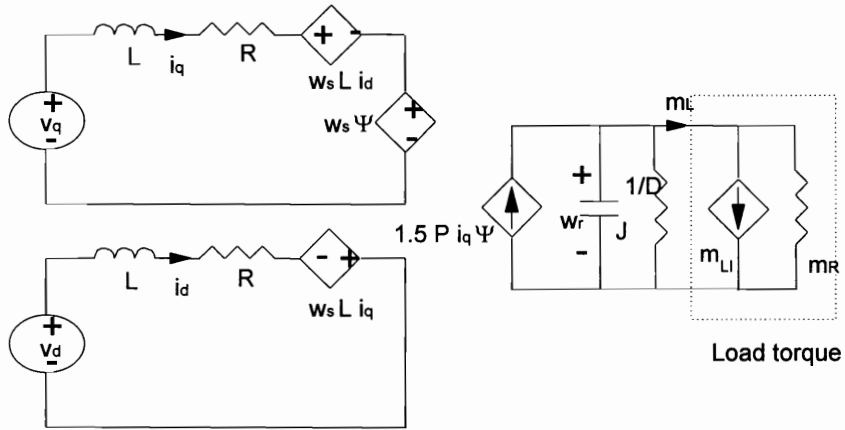
Load torque = m_L = m_{LI} + (w_r / m_R)

m_{LI} - Componenet of load torque that is independant of speed

m_R - Componenet of load torque that is dependant on speed

Figure 3.3 Large-signal Average Model of Permanent Magnet Synchronous Motor (PMSM) in d-q co-ordinates

the variables. By substituting equations (3.6) in (3.1)-(3.5), and linearizing, the small-signal model of PMSM is developed [8,9,10]. This small-signal model is shown in Figure 3.4 and will be used to analyze the input-impedance characteristics of PMSM.

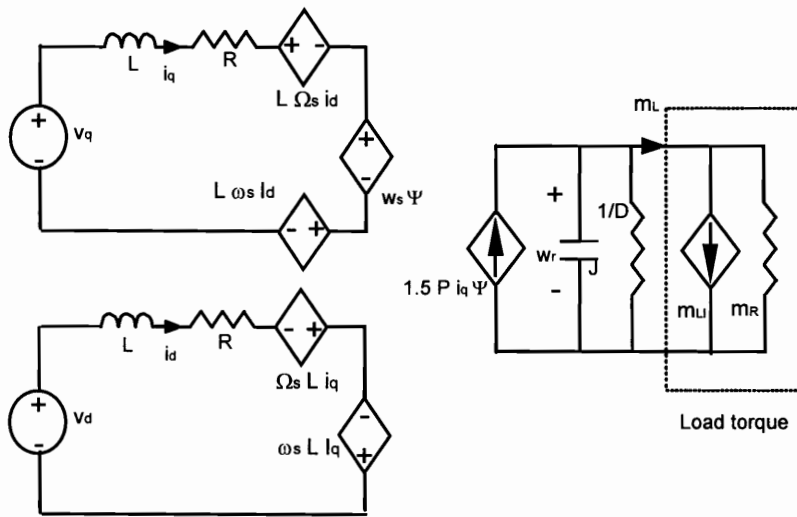### 3.2.2 Modeling of Three-Phase Voltage Source Inverter (VSI)

Three-phase voltage source inverter (VSI) is a popular inverter topology used because of simplicity in design and ease of control. The VSI used to drive a three-phase motor typically consists of switches only and a typical topology is shown in Figure 3.4.

At frequencies significantly lower than the switching frequency, the operation of the network can be modeled by an average model [14]. The d-q average large-signal model of the VSI obtained is shown in Figure 3.5 [14].

By perturbing and linearizing this model by a procedure similar to that discussed in the previous section (Section 3.2.1), the small-signal model of VSI is obtained. This model is used in conjunction with the small-signal model of PMSM to study the input impedance of the inverter-fed motor drive system shown in Figure 3.1.

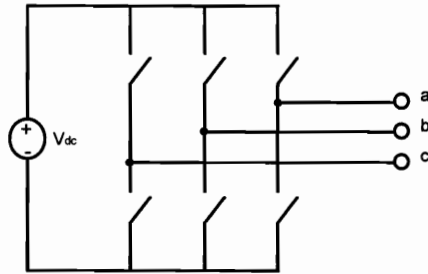### 3.3 Study of Input Impedance of Inverter-fed Motor Drive System

In Section 3.2, the PMSM and the voltage source inverter were modeled in d-q

Figure 3.4 Small-signal Average Model of Permanent Magnet Synchronous Motor (PMSM) in d-q co-ordinates

Figure 3.5 A typical three-phase voltage source inverter (VSI) topology

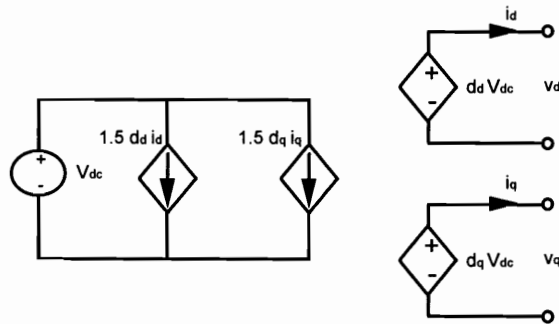**Figure 3.6 Large-signal Average Model for three-phase Voltage Source Inverter (VSI) in d-q co-ordinates**

Note: All Uppercase letters represent steady-state values of variables and all lowercase letters representsmall-signal perturbation in the variables.
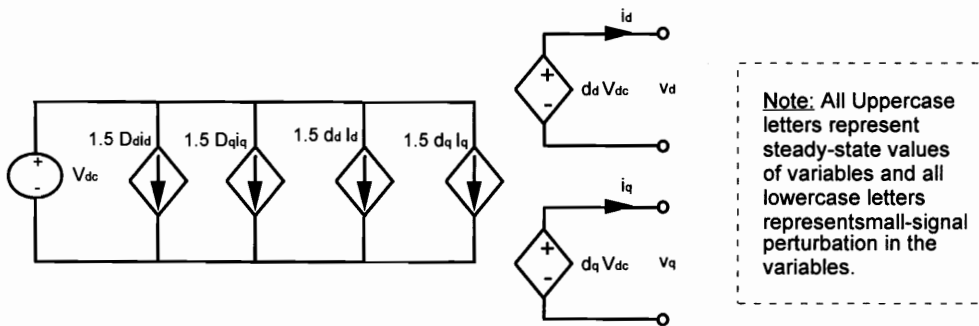
Figure 3.7 Small-signal Average Model for three-phase Voltage Source Inverter (VSI) in d-q co-ordinates

co-ordinates. Both the large signal model and small signal models were obtained. Using these models, the input impedance of the drive system will be studied.

In this section the system shown in Figure 3.8 will be considered for the study of input impedance characteristics. As can be seen this system consists only of the inverter and the motor. The small-signal models of the inverter and motor obtained by perturbing and linearizing the large-signal models shown in Figure 3.5 and 3.3 respectively are connected together as shown in Figure 3.9. Using this model the input impedance characteristics of the drive system will be studied.

3.3.1 Analytical Derivation of Input Impedance of Inverter-fed Motor Drive

When the drive system shown in Figure 3.8 is used in normal operation without any field weakening, the steady-state value of i_d, I_d will be maintained at zero. Also, to achieve this, D_d will have to be very low. Under this condition, an approximate analytical derivation can be made for the input impedance, Z_{IL} of the drive system shown in Figure 3.8.

$$Z_{IL} = \frac{v_{in}^p}{i_{in}^p}, \text{ with } m_L{}^p = 0.$$

After applying Kirchoff's voltage law to Figure 3.9, and simplification,

$$Z_{IL} = \left[\frac{s^2 + 2\delta w_2 s + w_2^2}{s + w_1} \right] \cdot \left[\frac{L}{1.5D_q^2} \right]$$

$$(3.7)$$
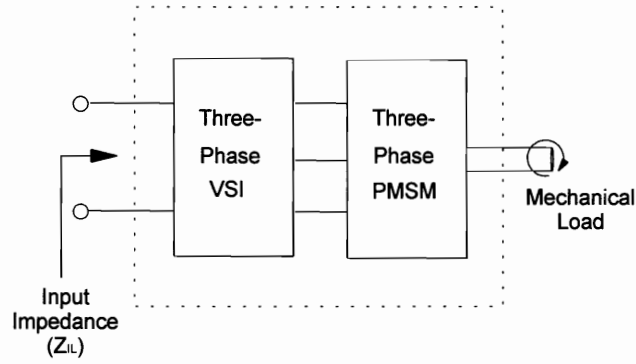
Figure 3.8 System used in Section 3.3 for Study of Input Impedance

Figure 3.9 Small-signal Model of System shown in Figure 3.8

where,

$$w_1 = \frac{D}{J}$$
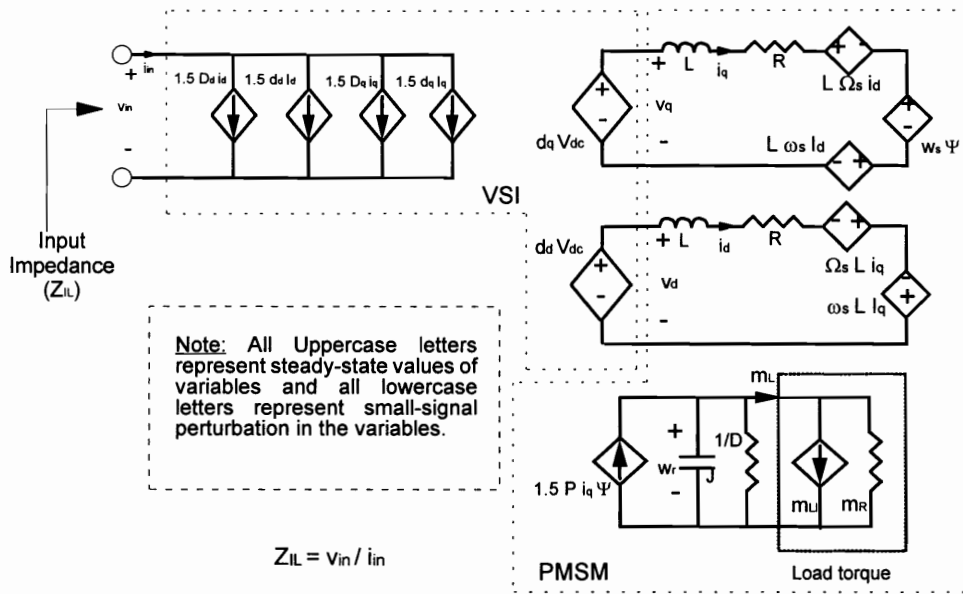
(3.8)

$$w_2 = P \ \Psi \ \sqrt{\frac{1.5}{L.J}}$$

(3.9)

$$\delta = \left[\sqrt{\frac{J}{1.5L}} \right] \left[\frac{R}{2P\Psi} \right]$$

(3.10)

Z_{ILDC}, the dc magnitude of the input impedance Z_{IL} is given by,

$$Z_{ILDC} = \left[\frac{P^2\Psi^2}{D} \right] \left[\frac{1}{D_q^2} \right]$$

(3.11)

As can be seen from equations (3.7)-(3.11) the input impedance (Z_{IL}) has one real pole and a pair of complex conjugate zeros. The location of the real pole is dependent on the moment of inertia (J) and the damping co-efficient (D). The frequency of the complex conjugate zeros is determined by the stator inductance of the PMSM (L), the moment of inertia (J), the number of pair of poles of PMSM (P), and the stator to rotor mutual linkage (Ψ). The damping of these complex

conjugate zeros is influenced by moment of inertia (J), stator inductance (L), stator resistance (R), the number of pair of poles of PMSM (P), and the stator to rotor mutual linkage (Ψ). The dc magnitude Z_{ILDC} is dependent on the damping co-efficient (D), the number of pair of poles of PMSM (P), and the stator to rotor mutual linkage (Ψ), and the q-axis duty cycle of the voltage source inverter (D_q). The input impedance (Z_{IL}) is not a function of the switching frequency of the voltage source inverter since this is an average model where the switching frequency information is eliminated [14]. This model assumes ideal switches in the voltage source inverter [14]. The on-resistance of the switches of the inverter (R_{on}) if any, will appear in series with the stator resistance (R) of the PMSM [14] in Figure 3.9. In order to include the effect of R_{on} on Z_{IL}, it is necessary to replace R by ($R+3*R_{on}$) in equations (3.8)-(3.12) [14]. The rest of this thesis will assume ideal switches in the VSI for simplicity of analysis. In cases where it is necessary it is easy to include it using the expression given above.

3.3.2 Computer Simulation of Input Impedance of Inverter-fed Motor Drive

This model was implemented in the simulation software EASY5x [15]. By applying small-signal perturbation in input voltage v_{in}, the input impedance was studied, using equation (3.7).

The typical input impedance characteristics are shown in Figure 3.11 for a PMSM rated at 3kW. The parameters of the PMSM are shown in Figure 3.10.

Parameters of PMSM used in Figure 3.9 are [16]:

Motor type: High Performance/ High Torque PMSM
Manufacturer: Inland Motor/ Kollmorgen Corporation
Motor Model: RBE (H) 06200 Series
Peak Rated Torque: 90 N-m
Power at Peak Rated Torque: 1.2 kW
Max. Continuous Output Power: 3.12kW
L= 1.9 mH
R= 0.18
Ψ= 1.21 V/ (rad/sec)
ws = 150 rad/sec
mL = 20 N-m
D= 0.0044 N-m/rad/sec
J= 0.023 kg-m2
P= 1

Figure 3.10 Parameters of PMSM used in Figure 3.9
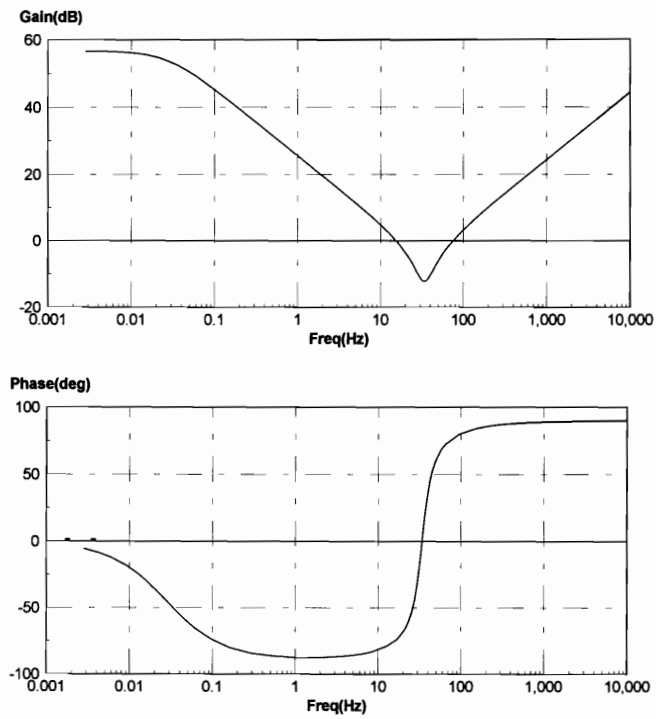
Figure 3.11 Typical Input Impedance Characteristics of Inverter-fed PMSM Drive shown in Figure 3.8

From Figure 3.11 it is also seen that the input impedance (Z_{IL}) consists of one real pole around 0.03 Hz and a pair of complex zeros around 35 Hz. It is also seen that the phase of input impedance stays between -90 degrees and +90 degrees over the entire frequency range.

It can be seen from equation (3.10) that the double pole of the drive system is caused by the resonance between the stator inductance (L) of PMSM, an electrical parameter and the moment of inertia (J), a mechanical parameter. Hence this resonance is an electromechanical resonance and this occurs around 35 Hz for the motor considered.

3.3.3 Computer Simulation of Input Impedance of the Complete Inverter-fed Motor Drive System

The previous two sections (Sections 3.3.1 and 3.3.2) studied the input impedance characteristics of the drive system shown in Figure 3.8, consisting only of inverter and motor. In this section the input impedance of the drive system shown in Figure 3.1, containing EMI filter, inverter and motor will be studied through computer simulation. The EMI filter topology shown in Figure 3.2 is used for the EMI filter. The detailed design of EMI filter is given in Appendix B. A typical voltage source inverter switching at 20kHz [17] is assumed. Also the voltage source inverter is capable of supplying the power of 3kW demanded by

the PMSM given in Figure 3.10. The input DC voltage to the VSI is assumed to be 120 V. The resulting values of the EMI filter components are:

$$L_1 = 21 \ \mu H$$

$$L_2 = 5 \ \mu H.$$

$$C_1 = 540 \ \mu F.$$

$$C_2 = 100 \ \mu F.$$

$$R_1 = 0.2 \ \Omega.$$

Figure 3.12 shows the input impedance of the drive system shown in Figure 3.1. It can be seen that the input impedance has two resonances: a low frequency electromechanical resonance due to PMSM, and a high frequency resonance due to the EMI filter. Thus the input impedance of the inverter-fed motor drive system operating without speed regulation is determined by the PMSM at low frequencies and the EMI filter at high frequencies. It is also seen that the phase of this input impedance also always stays between -90 and +90 degrees.

3.3.4 Study of Input Impedance of Inverter-fed PMSM Drive operating with Speed Regulation

In the previous three sections (Sections 3.3.1, 3.3.2 and 3.3.3) the input impedance characteristics of the inverter-fed PMSM drive operating without speed regulation was studied. In this section the inverter-fed PMSM drive with

41
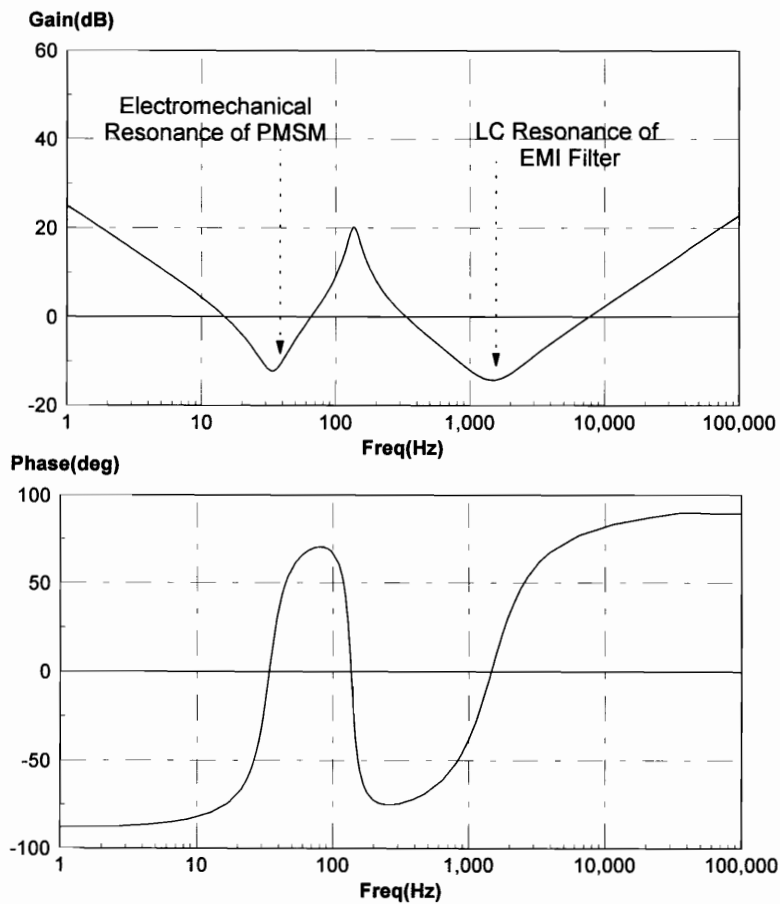
Figure 3.12 Typical Input Impedance Characteristics of the Complete Inverter-fed PMSM Drive shown in Figure 3.1

speed regulation will be studied. This requires a speed feedback loop as shown in Figure 3.13. In this figure, the closed-loop control is implemented by the field-oriented control method [8,17]. This system was set up in EASY5x and the input impedance characteristics was simulated for the following closed loop design [17].

$$H(s) = \frac{9.25(s + 72)}{s}$$

$$C(s) = \frac{0.018(s + 55.5)}{s}$$

$$K_d = 0.2$$

The design of the feedback loop is discussed in detail in [17]. The input impedance characteristics for this system is shown in Figure 3.14. As can be seen, the electromechanical resonance has been suppressed by the closed loop control. The EMI filter resonance is still seen. However, the phase of input impedance ranges from -180 degrees to +90 degrees for this case. At low frequencies the phase is -180 degrees and high frequencies the phase is +90 degrees. Hence, the input impedance of the inverter-fed motor drive system operating with speed regulation is dominated predominantly by the EMI filter.

3.3.5 Review of Input Impedance Characteristics of Resistive and Power Supply Loads
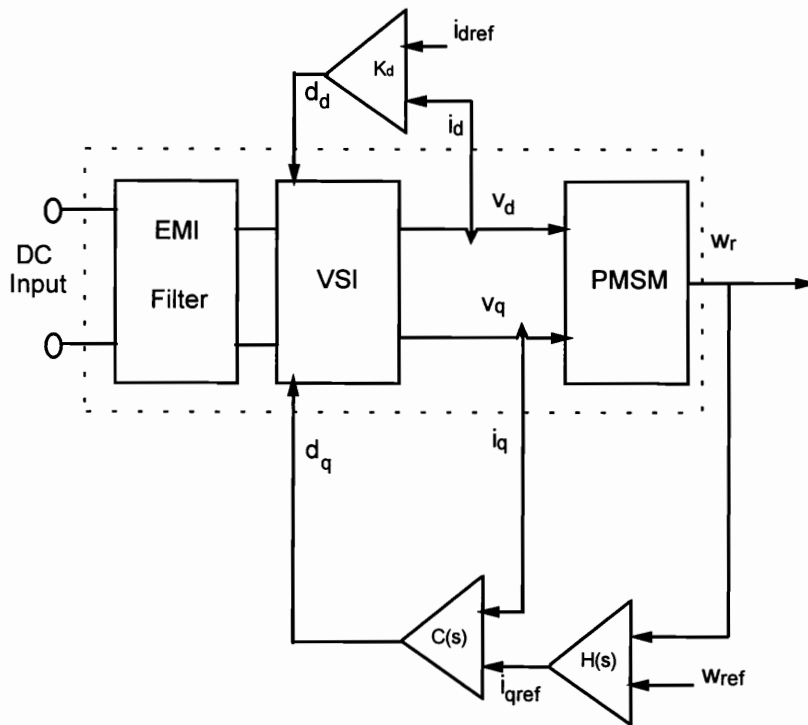
Wref - Reference Speed
idref - Reference d- axis current
H(s) - Speed Loop PI Controller
C(s) - q-axis Current Loop PI Controller
Kd - d-axis P Controller Gain

Figure 3.13 Inverter-fed PMSM Drive Operating with Speed Regulation
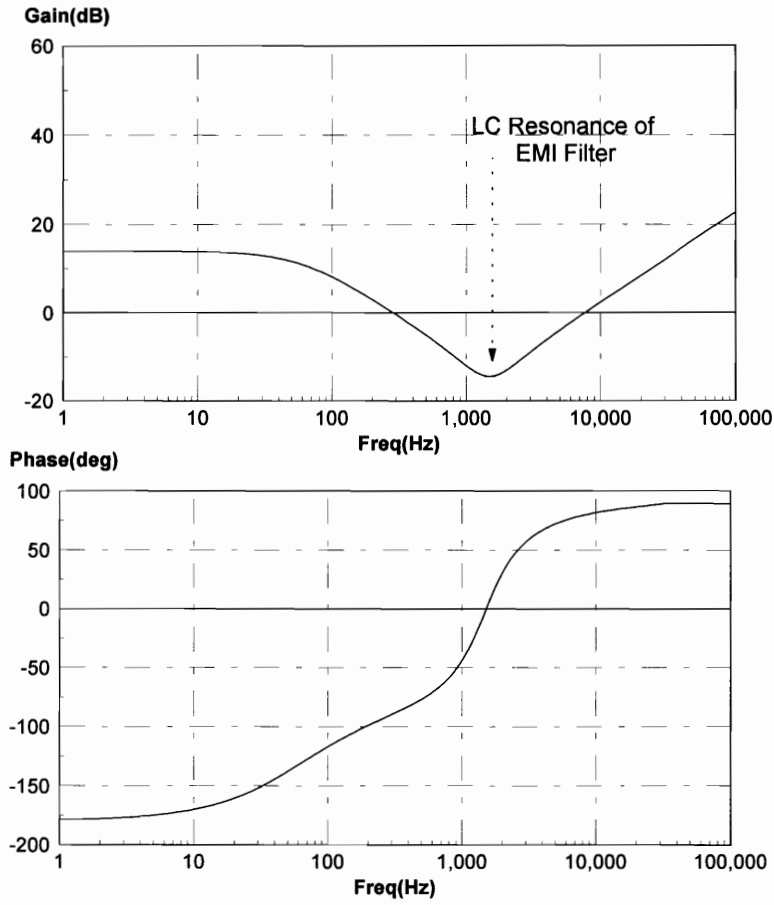
Figure 3.14 Typical Input Impedance Characteristics of the Inverter-fed PMSM Drive with Speed Regulation Shown in Figure 3.11

3.3.5.1 Resistive Loads

Resistive loads represent heater loads among other loads. They have been modeled and their input impedance characteristics have been analyzed in the past [3,5,11,12]. The typical input impedance characteristics of a 3kW resistive load Figure 3.15. The EMI filter used has the following parameter values:

$$L_1 = 21 \ \mu H$$

$$L_2 = 5 \ \mu H.$$

$$C_1 = 540 \ \mu F.$$

$$C_2 = 100 \ \mu F.$$

$$R_1 = 0.2 \ \Omega.$$

The resistive load connected to the output of the EMI filter has a value of :

$$R_{load} = 4.8 \ \Omega.$$

It can be seen that the magnitude of input impedance is dominated by the EMI filter only. Also, the phase is between -90 and +90 degrees over the entire frequency range. At low frequencies the phase is 0 degrees and at high frequencies the phase is +90 degrees. It is observed that the input impedance of a resistive is load is dominated predominantly by the EMI filter.

3.3.5.2 Power Supply Loads

Regulated switching power supply loads have been modeled and their input impedance has been studied in the past [3,5,11,12]. It has been shown that these

Figure 3.15 Typical Input Impedance Characteristics of Resistive and Power Supply Loads

loads can be represented adequately by a negative resistance load for small-signal purposes. The input impedance of a typical power supply load operating at 3kW is shown in Figure 3.15. The EMI filter used has the following parameter values:

$$L_1 = 21 \ \mu H$$

$$L_2 = 5 \ \mu H.$$

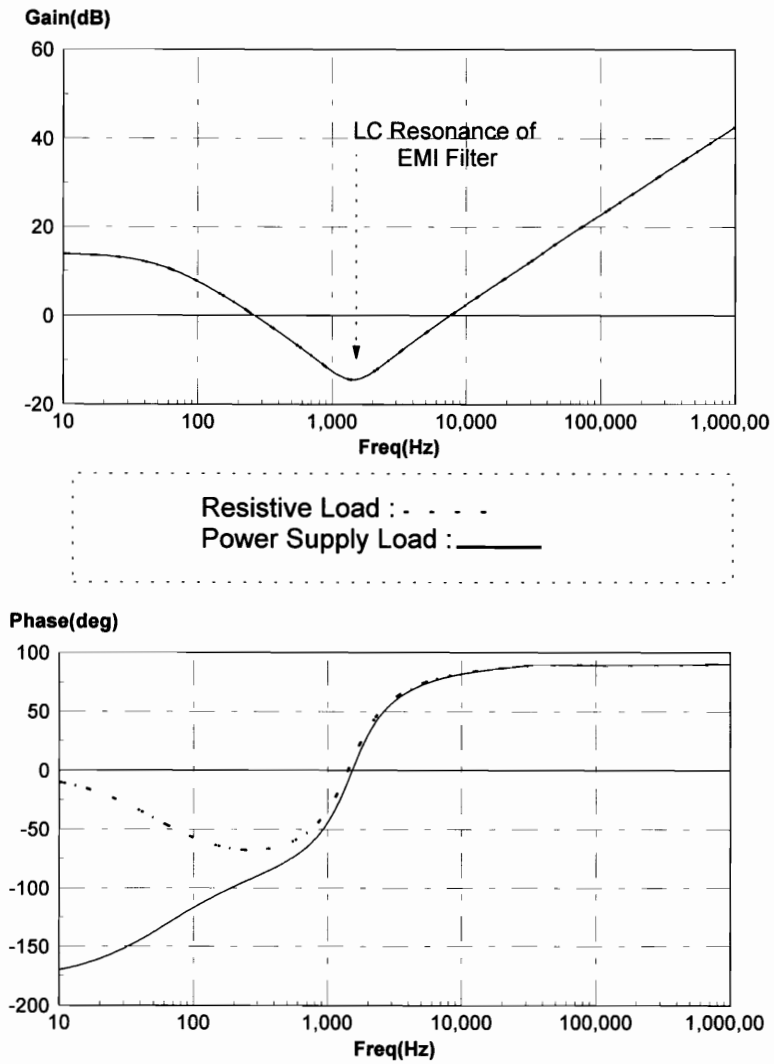$$C_1 = 540 \ \mu F.$$

$$C_2 = 100 \ \mu F.$$

$$R_1 = 0.2 \ \Omega.$$

The resistive load connected to the output of the EMI filter has a value of :

$$R_{load} = -4.8 \ \Omega.$$

It can be seen that the input impedance magnitude again is dominated only by the EMI filter. However, the phase ranges from -180 degrees to +90 degrees. The phase changes from -180 degrees at low frequencies to +90 degrees at high frequencies. It may be seen that this input impedance characteristics are very similar to that of the inverter-fed motor drive system shown in Figure 3.13. The input impedance of power supply loads are dominated by the EMI filter.

3.4 Summary

The inverter-fed motor drive system was modeled in d-q co-ordinates. Both the large-signal and small-signal models were obtained. Using these models the

input impedance characteristics of the drive system was studied both through computer simulation and analytical derivation. The input impedance of the drive system was studied for two operating modes: i) operation without speed regulation, and ii) operation with speed regulation. The input impedances of other well-known loads, namely resistive, and power supply loads were reviewed. It was observed that the inverter-fed drive system operating without speed regulation has a unique input impedance characteristics in that two resonances: one at a lower frequency (35 Hz) due to electromechanical resonance of PMSM and the second at a higher frequency (1400 Hz) due to LC resonance of EMI filter are present. This input impedance is different from that of the other well-known loads which have only one resonance in their input impedance. Also the input impedance of the drive system operating without speed regulation is dominated both by the PMSM and the EMI filter, whereas the input impedance of the other loads is dominated predominantly by the EMI filter. However, the inverter-fed motor drive system operating with speed regulation was found to have input impedance characteristics similar to that of power supply loads in both magnitude and phase.

CHAPTER 4

DESIGN ISSUES IN DESIGNING AN INVERTER-FED MOTOR DRIVE

SYSTEM FOR DPS APPLICATIONS

4.1 Introduction

In Chapter 3 the inverter-fed motor drive system was modeled and the input impedance characteristics were studied. It was observed that the inverter-fed motor drive system operating without speed regulation had an input impedance characteristics that was different from the input impedance of other well studied loads. This was due to the low frequency electromechanical resonance of the PMSM. It was also observed that when closed loop control was employed for speed regulation of the drive system, these electromechanical resonance was

suppressed and the input impedance of the drive system became identical to that of constant power loads.

In this chapter the effect of the unique input impedance characteristics of the motor drive system operating without speed regulation, on the performance and stability of the distributed power system (DPS) is studied. It is shown that in designing a load subsystem of this nature additional precautions that are not usually taken when designing other well-known loads (constant power loads, resistive loads) for use in DPS, should be taken to avoid interaction of the drive system with the source subsystem. Design guidelines are developed to help in designing the inverter-fed motor drive system of Figure 3.1, so that the performance and stability of the DPS is minimally affected by the unique input impedance of the drive system being studied. Figure 4.1 shows the block diagram of a two-stage DPS having the inverter-fed motor drive system as a load subsystem. The load subsystem consists of three blocks namely, the motor (PMSM), the inverter (VSI) and the EMI filter. Design guidelines will be developed for these blocks in the aforementioned sequence. A DC-DC converter that is a variation of the converter shown in Figure 2.2, will be used as the source subsystem throughout this chapter. The parameters that have been changed from Figure 2.2 are: $K_m = 300$; $w_{Z2} = 1150$; $L = 100$ μ H.

The output impedance magnitude and phase of this DC-DC converter are shown in Figure 4.2. It will be assumed that the source subsystem has already been
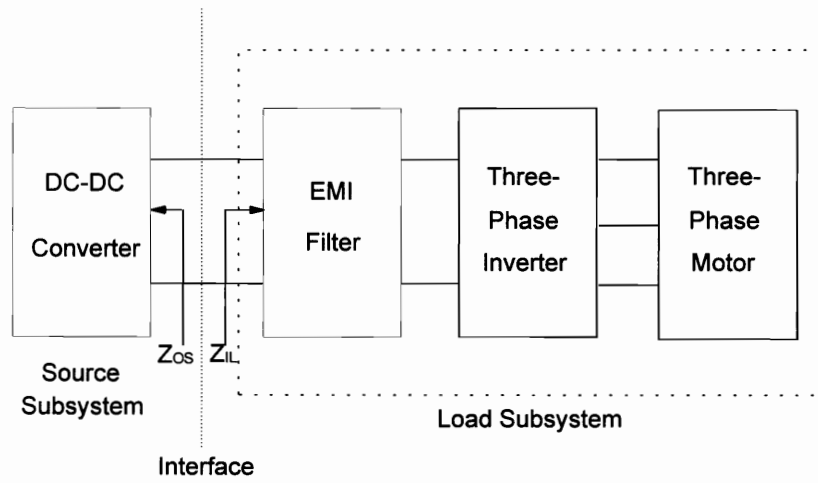
**Figure 4.1 A DPS with an Inverter-fed Motor Drive
System as Load Subsystem**
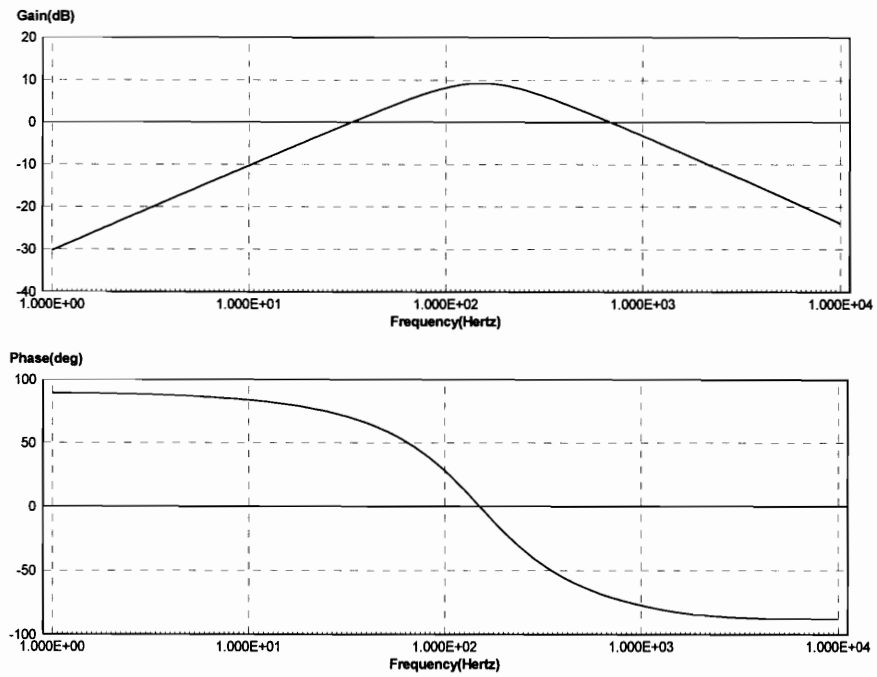
**Figure 4.2 Output Impedance (Z_{OS}) of the DC-DC Converter
used as Source Subsystem**

designed; and design guidelines will be developed for the motor drive subsystem that is to be connected to the source subsystem.

4.2 Design of Motor (PMSM)

It was shown in Section 3.3.3 that the input impedance of the inverter-fed motor drive system shown in Figure 4.1 when operating without speed regulation is determined at low frequencies by the electromechanical resonance of PMSM and at high frequencies by the LC resonance of the EMI filter. In Sections 2.4 and 2.5 it was shown that in order to ensure minimal interaction between the source and the load subsystems, i) the magnitude of the input impedance of the load subsystem ($|Z_{IL}|$) should not intersect the magnitude of the output impedance of the source subsystem ($|Z_{OS}|$), or ii) when there is an intersection between $|Z_{IL}|$ and $|Z_{OS}|$, the difference between the phases of Z_{OS} and Z_{IL} in the frequency range where $|Z_{IL}|$ and $|Z_{OS}|$ overlap should be less than 180 degrees. This condition ensures small signal stability of the integrated system. In addition it was shown that in order to avoid susceptibility to large signal instability the difference in phase should be sufficiently less then 180 degrees.

4.2.1 PMSM without speed regulation

It was shown in Chapter 3 that the inverter-fed PMSM drive operating without speed regulation is different from the other well-known loads in that the input impedance of the drive is determined both by the PMSM and the EMI filter; whereas the input impedance of the other well-known loads is determined predominantly by the EMI filter. In this chapter it will be analyzed to see whether the unique electromechanical resonance characteristics of the motor (PMSM) will lead to any interaction problems with the source subsystem that might deteriorate the DPS performance.

Two motors (PMSM) with the parameters shown in Figure 4.3 are considered as examples. Motor #1 and Motor #2 have very similar torque, speed and power ratings. Both of them also have similar parameters except moment of inertia (J) and stator inductance (L). Motor #1 has a higher moment of inertia (0.045 kg-m^2) than Motor #2 (0.005 kg-m^2), while Motor #2 has a higher stator inductance (8.5 mH) than Motor #1 (3.8 mH). Using these two motors, two Load subsystems are formed as shown in Figure 4.4. Figure 4.5 shows the output impedance of the source subsystem (Z_{OS}) compared to the input impedances (Z_{IL1}, Z_{IL2}) of these two load subsystems. It is seen that Motor #2 which has a higher stator inductance and a lower moment of inertia has a higher input impedance magnitude.

Now a load torque transient is applied to the system as shown in Figure 4.4. The transient response of the output voltage of the source subsystem is shown in Figure 4.6 for the two load subsystems formed by the two aforementioned loads. It can be seen that the system formed with Motor #1 in the load subsystem has sustained oscillations in the output voltage. The system formed with Motor #2 however has a stable transient response.

Parameters of the two PMSMs used in Section 4.2 are [16]:

Motor #1

Motor type: High Performance PMSM
Manufacturer: Inland Motor/ Kollmorgen Corporation
Motor Model: RBE (H) 04500 Series
Peak Rated Torque: 60 N-m
Power at Peak Rated Torque: 1.5 kW
Max. Continuous Output Power: 3.1kW
L= 3.8 mH
R= 0.19
Ψ= 1.2 V/ (rad/sec)
ws = 150 rad/sec
mL = 20 N-m
D= 0.0046 N-m/rad/sec
J= 0.045 kg-m2
P= 1

Motor #2

Motor type: High Performance PMSM
Manufacturer: Inland Motor/ Kollmorgen Corporation
Motor Model: RBE (H) 04500 Series
Peak Rated Torque: 55 N-m
Power at Peak Rated Torque: 1.5 kW
Max. Continuous Output Power: 3kW
L= 8.5 mH
R= 0.19
Ψ= 1.2 V/ (rad/sec)
ws = 150 rad/sec
mL = 20 N-m
D= 0.01 N-m/rad/sec
J= 0.005 kg-m2
P= 1

Figure 4.3 Parameters of PMSM used in Section 4.2
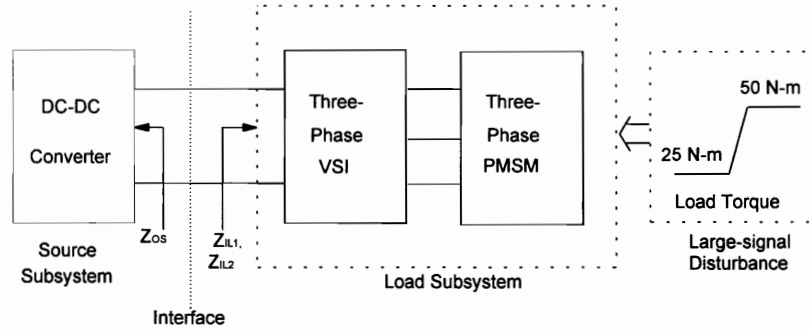
Figure 4.4 Integrated System (DPS) used for Study of the Influence of PMSM on DPS in Section 4.2
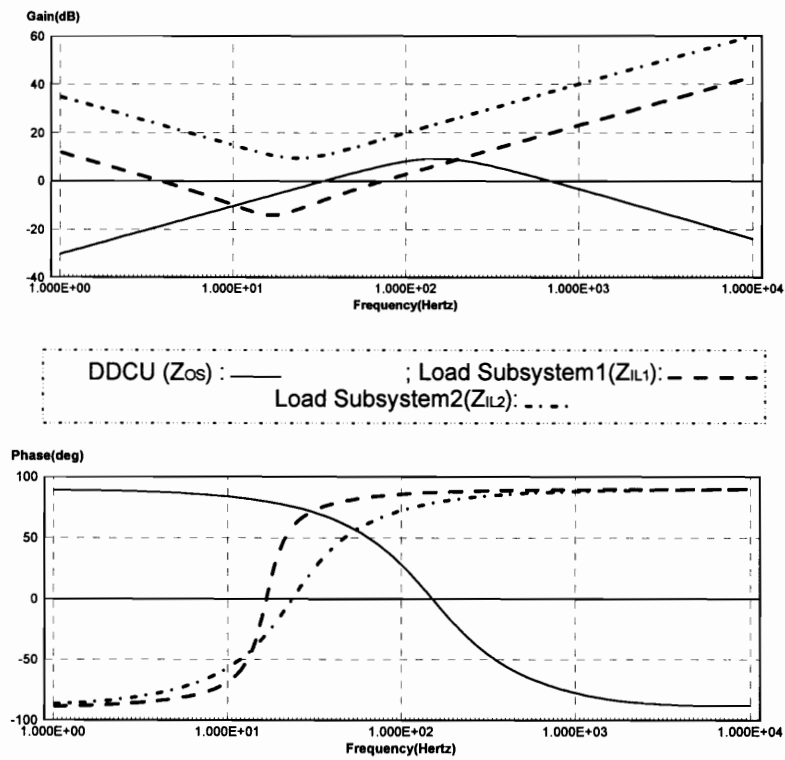
Figure 4.5 Output Impedance (Z_{OS}) of the Source Subsystem Compared to Input Impedances (Z_{IL1}, Z_{IL2}) of two PMSM Drive Load Subsystems without EMI Filter
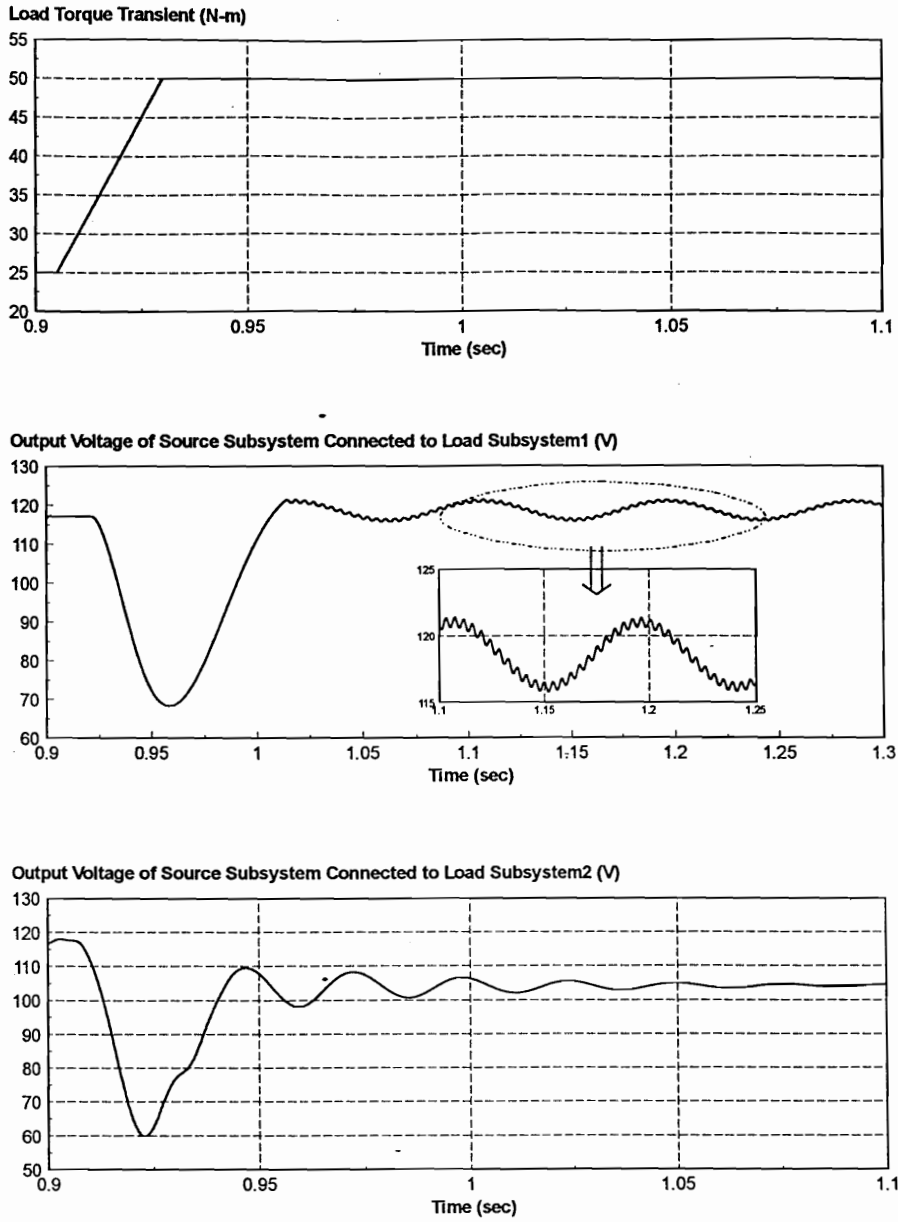
Figure 4.6 Transient Response of the Integrated System (DPS) Formed by Connecting the Two Load Subsystems with the Source Subsystem

This can be explained by observing Figure 4.5. It can be seen that $|Z_{OS}|$ and $|Z_{IL1}|$ intersect, and at the point of intersection (10Hz), the phase difference between Z_{OS} and Z_{IL1} is approximately 159 degrees. This means a phase margin of only 21 degrees for T_M, and hence the resulting transient is oscillatory and excites the non-linearities in the system namely the duty cycle saturation in the DC-DC converter, and leads to instability. The oscillation has a frequency of 10 Hz and a magnitude of about 5 volts as shown in Figure 4.6. Another oscillation at a frequency of around 150 Hz is riding at the top of this oscillation and has a magnitude of about 0.75 V. This is due to the second intersection of $|Z_{OS}|$ and $|Z_{IL1}|$ that occurs around 150 Hz as shown in Figure 4.5. However $|Z_{OS}|$ and $|Z_{IL2}|$ are well separated over the entire frequency range and this means that the load subsystem minimally affects the performance of the integrated system (DPS) shown in Figure 4.4.

From the above example it is seen that in an application where PMSM is used without speed regulation loop, a motor that gives the highest possible input impedance magnitude for a given application should be selected, in order to give the best possible performance of the DPS. A series of simulations were run to study the input impedance of the inverter-fed PMSM drive shown in Figure 4.4, for different parameter values of PMSM. A representative set is shown in Figure 4.7. Motor #1 and Motor #2 have the parameter values as given by Figure 4.3. From the Figure 4.5 and the discussion in Section 3.3, it can be seen that in order to ensure a high input impedance of the inverter-fed PMSM drive shown in Figure 4.4 operating without speed regulation, the PMSM should have:

i) Lowest possible moment of inertia;

ii) Highest possible stator inductance;

iii) Highest possible stator resistance.

The same conclusion can be drawn by studying equations (3.7)-(3.11) as well. In the above three conditions, having a high stator resistance (R) leads to copper losses in the stator winding and heating of the motor and hence is not practical.

Hence, the design guidelines for designing (selecting) the PMSM in an application where it is used without speed regulation loop, and as a part of the load subsystem of the DPS can be summarized as follows.

Design Guidelines:

i) From the foregoing example with two motors whose parameter values are given in Figure 4.3 it was shown that a PMSM with a lower moment of inertia has a higher input impedance. For the same weight of the rotor, a motor with a rotor of smaller diameter will have a lower moment of inertia than one with a rotor of larger diameter [19]. Motor manufacturers like Inland motors [16] make motors of same power, speed and torque ratings available with different values of moment of inertia [16]. A PMSM with a low moment of inertia (J) should be selected.

ii) In the forgoing example it was seen that a PMSM with a higher stator inductance has a higher input impedance. Having selected a motor with a low moment of inertia, it is necessary to make sure that it has a high enough stator inductance (L) so that the input impedance due to PMSM will meet Criterion 2.1 (page 21). Motor manufacturers [16] also make motors of same power, speed and torque ratings available with different values of stator inductance [16]. [16] also

mentions that custom windings can be fitted in their PMSM according to the specification of the buyer to tailor among other parameters, the stator inductance. Hence a motor with as high a stator inductance as needed to ensure that the input impedance due to the PMSM, when compared to the output impedance of the source subsystem satisfies Criterion 2.1 (page 21) should be selected (designed), if such a motor design is practical.

iii) If a practical motor design does not yield the value of stator inductance (L) needed to satisfy Criterion 2.1 (page 21), then external inductances should be connected in series with the three phases of the stator winding to ensure that Criterion 2.1 (page 21) is satisfied as explained above.

4.2.2 PMSM with speed regulation

In the previous section a motor drive operating without speed regulation was studied. Now, the inverter-fed motor drive operating with a speed regulation loop as shown in Figure 3.13 will be used to replace the load subsystem shown in Figure 4.4. Again, for the purposes of study in this section, the EMI filter will be ignored. It was seen earlier in this section that Motor #1 when used without speed regulation loop, leads to instability in the DPS formed by interconnecting the source subsystem to the load subsystem where this motor is used. Now, Motor #1 will be used with the speed regulation loop discussed in Section 3.3.4 to form the load subsystem. A detailed discussion of speed feedback loop design can be found

Gain(dB)

Frequency(Hertz)

Motor #1 : _ _ _ _   ; Motor #2: _ . _ . _

Phase(deg)

Frequency(Hertz)
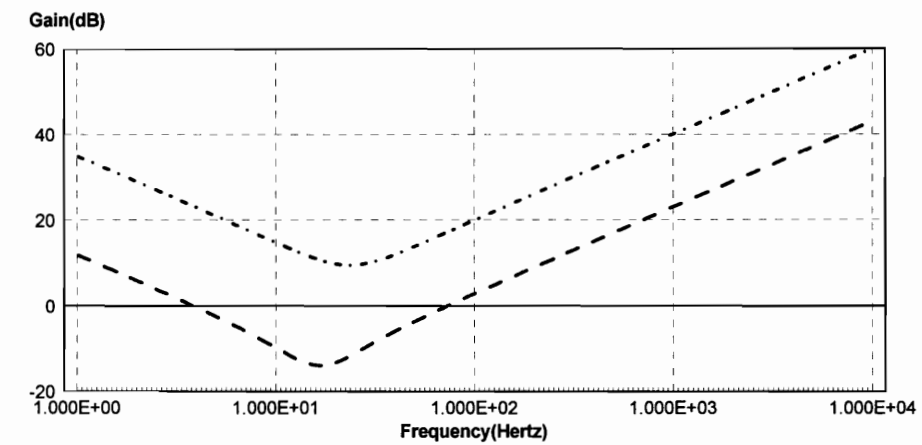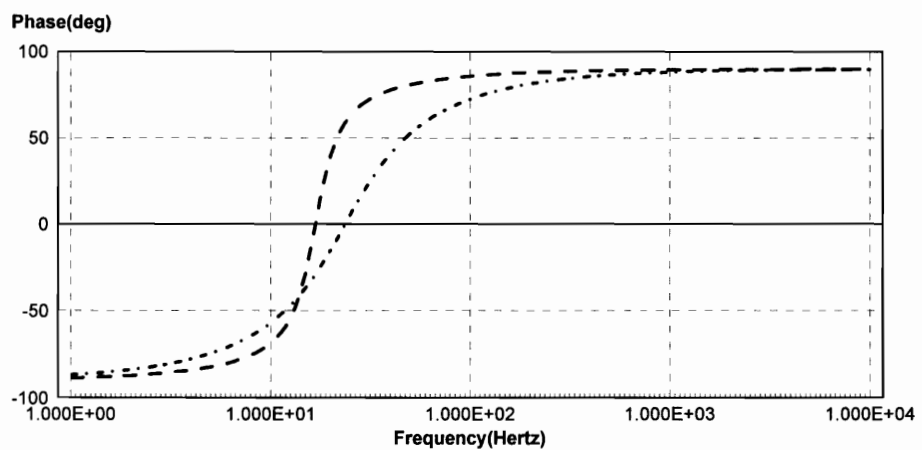
**Figure 4.7 Comparison of Input Impedances of Inverter-fed
PMSM Drive Systems Shown in Figure 4.4 for Different
Parameters of PMSM**

Gain(dB)

Phase(deg)

DDCU (Z$_{OS}$) : ——— ; Load Subsystem(Z$_{IL}$): - - - -
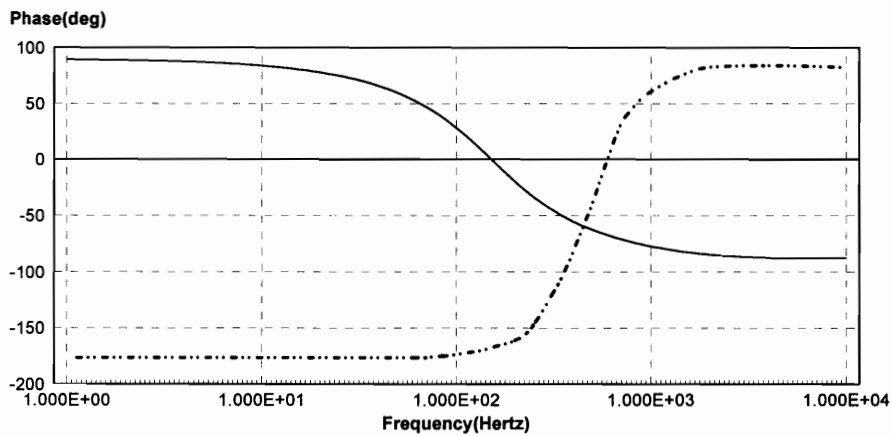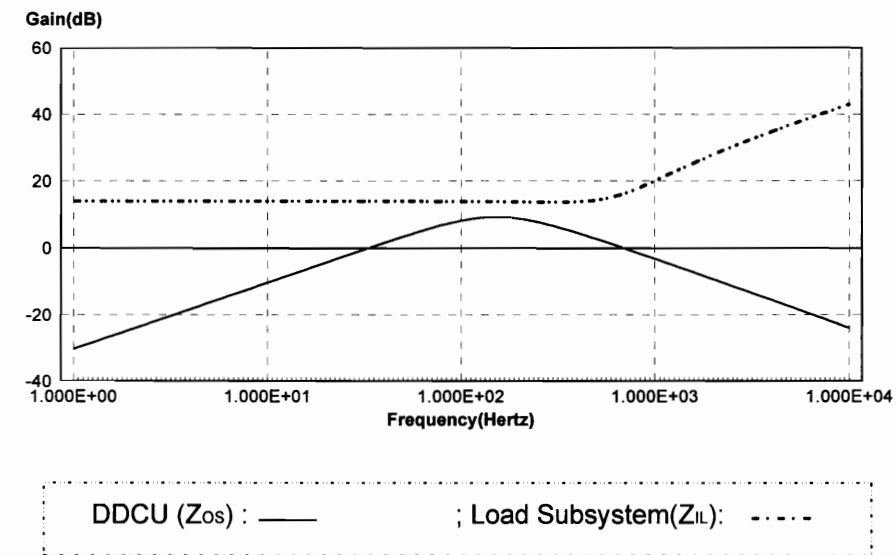
**Figure 4.8 Output Impedance (Z$_{OS}$) of the Source Subsystem
Compared to Input Impedance(Z$_{IL}$) of PMSM Drive Operating
with Speed Regulation and without EMI Filter**

in [17]. Figure 4.8 shows the input impedance of the inverter-fed PMSM drive operating with speed regulation (Z_{IL}) compared against the output impedance of the source subsystem (Z_{OS}). It is seen that the electromechanical resonance seen in Figure 4.5 is suppressed by the closed loop control employed. Hence $|Z_{IL}|$ and $|Z_{OS}|$ do not intersect. The transient output voltage of the source subsystem when the DPS is subjected to a load torque transient is shown in Figure 4.9. It can be seen that this is stable as against the instability that resulted when using the same motor drive system without speed regulation loop.

Hence, while the PMSM is operating with the speed regulation loop designed according to [17], the electromechanical resonance in the input impedance of the motor (PMSM) drive load subsystem will be suppressed, and hence does not cause interaction problems with the source subsystem as discussed earlier in this section.

4.3 Design of Inverter (VSI)

The voltage source inverter (VSI) topology is shown in Figure 3.5. It can be seen that it consists of only switching elements. Thus the practical design of voltage source inverter consists of: i) selecting the switching elements and designing the associated circuitry like driver circuits, snubbers etc. and ii) selecting the switching frequency. There is no significant influence on the input
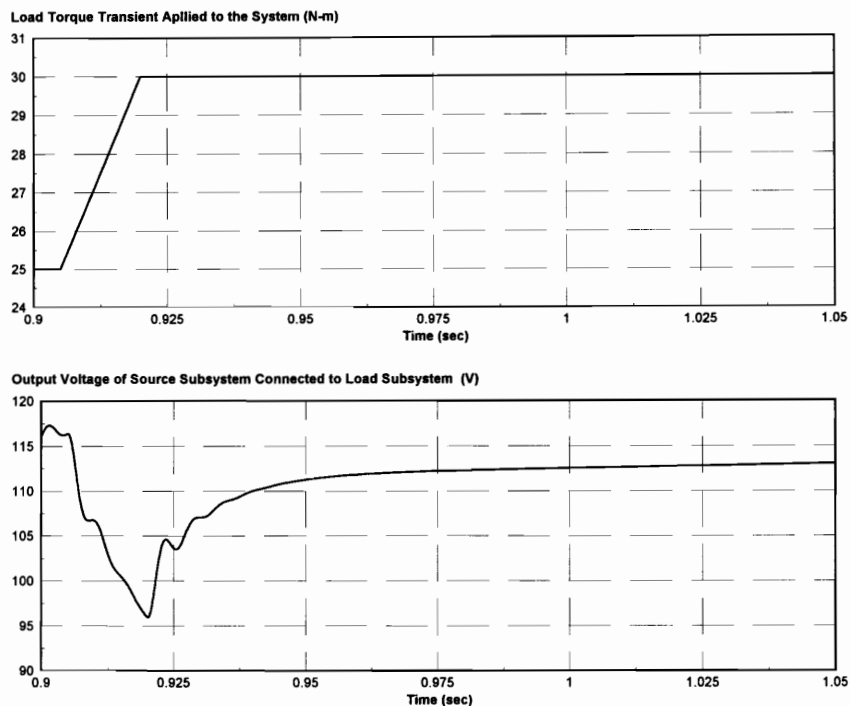
**Figure 4.9 Transient Response of the Integrated System (DPS)
Formed by Connecting the Inverter-fed Motor Drive
operating with Speed Regulation with the Source Subsystem**
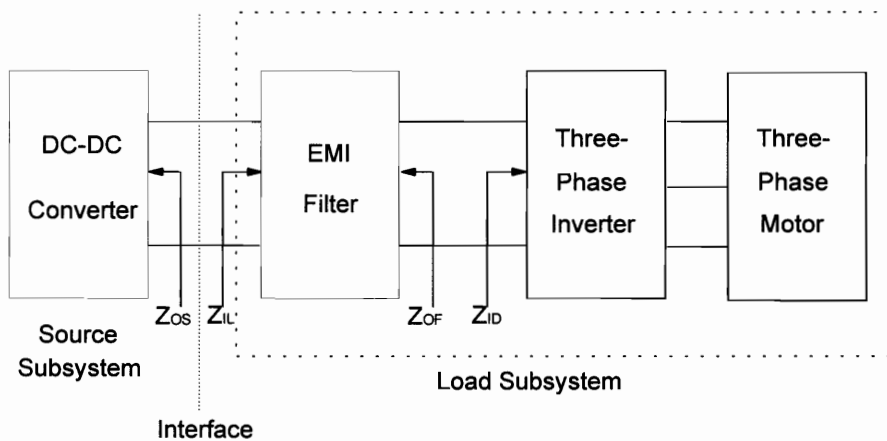
**Figure 4.10 A DPS with an Inverter-fed Motor Drive
System as Load Subsystem studied in Section 4.4**

impedance of the load subsystem and hence the performance and stability of the integrated DPS, by the first step mentioned above. However, the selection of the switching frequency (f_s) of the inverter does affect the input impedance of the load subsystem and hence the performance of the integrated DPS.

The switching frequency (f_s) of the inverter does not affect the shape of the input impedance of PMSM since the small signal model used is an averaged model and thus eliminates the switching frequency information [14]. However once the PMSM is selected (designed) as explained in Section 4.2, the design of the switching frequency of the inverter determines the magnitude of the ripple current drawn from the source by the inverter-fed PMSM drive, as well as the frequency of this ripple current (which is at switching frequency). Both of these parameters affect the design of the front end EMI filter for the load subsystem as described in Appendix B. As seen in Section 3.3 the front end EMI filter of the load subsystem contributes the LC resonance in the input impedance of the load subsystem shown in Figure 3.12. This directly affects the performance and stability of the DPS as explained in the following Section, Section 4.4. The switching frequency of the inverter which in typical designs is a few tens of kHz [17] does not affect the input impedance of load subsystem or the performance and stability of the DPS in any other way. Hence the design guidelines for designing the switching frequency of the voltage source inverter can be summarized as follows.

Design Guidelines:

i) The switching frequency of the voltage source inverter should be designed such that it is possible to design the front end EMI filter following the procedure in Appendix B to meet the design guidelines given in Section 4.4.

ii) If the switching frequency of the inverter is higher for the same PMSM design and same source, it means a lower magnitude input ripple current that is at a higher frequency [17]. For such a case it is easier to design an EMI filter to meet the design guidelines given in Section 4.4, as explained in the next section.

iii) So, the switching frequency of the inverter should be designed to be high enough so that it is practical to design the front end EMI filter for the load subsystem following the guidelines in Section 4.4 and the procedure in Appendix B.

4.4 Design of EMI Filter

The primary purpose of the EMI filter is to attenuate the switching frequency ripple in the current drawn by the VSI, so that the rest of the system is not affected badly due to the electromagnetic interference caused by the high frequency ripple waveform [1,18]. However, when designing an EMI filter for use as the input filter of a load subsystem to be used in a DPS, it is imperative to design the EMI filter so that the input impedance of the EMI filter, does not interact with the

output impedance of the source subsystem [1,4,5,12,18]. In designing the EMI filter to be used as input filter of an inverter-fed motor drive load subsystem, it is important to take into account more criteria which will be discussed in the rest of this section.

4.4.1 Interaction between the EMI Filter and the Inverter-fed Motor Drive

Figure 4.10 shows the block diagram of the system to be studied in this section. Apart from the attenuation of switching frequency ripple, the first point to take into account when designing the EMI filter for use as an input filter of an inverter-fed motor drive system operating without speed regulation, is to make sure that the output impedance of the EMI filter (Z_{OF}) does not interact with the input impedance of the inverter-fed motor drive system (Z_{ID}). As discussed in Section 3.3, the input impedance of the inverter-fed PMSM has an electromechanical resonance that leads to a drop in the magnitude of the input impedance; however, this resonance typically occurs at frequency of a few tens of Hz. Also, typical designs of EMI filters as shown in Section 3.2, have an LC resonance occurring at a frequency around 1kHz. Hence, generally the frequencies of peaking in the output impedance of EMI filter (Z_{OF}) and that in the input impedance of motor drive (Z_{ID}) are well separated. However, if particular attention is not paid, a design of EMI filter can lead to an overlap between $|Z_{OF}|$ and $|Z_{ID}|$, and if the difference between their phases is close to 180 degrees, then

the system will have a small phase margin in small-signal sense. This might lead to large-signal performance degradation of the DPS or even large-signal oscillations as explained in Chapter 2. In this section two example filter designs, Filter #1 and Filter #2 are used to demonstrate the way in which a bad design of EMI filter might lead to non-minimal interaction between the filter and the inverter-fed PMSM. Both Filter#1 and Filter#2 are designed in order to get the necessary attenuation in the input current ripple as explained in Appendix B. Since there is only one design constraint (desired attenuation at the switching frequency) and multiple design parameters (L_1, L_2, R_1, C_1, and C_2) the constraint can be satisfied with different sets of component values. Two such designs are:

Filter #1: $L_1 = 3$ mH; $L_2 = 55$ μH; $R_1 = 3$; $C_1 = 55$ μF; $C_2 = 10$ μF.

Filter #2: $L_1 = 0.45$ mH; $L_2 = 55$ μH; $R_1 = 0.3$; $C_1 = 360$ μF; $C_2 = 10$ μF.

It can be seen from Figure 4.11 that in case of Filter #1, the input impedance of the motor drive and output impedance of EMI filter (Z_{OF1}) overlap. The motor used in this example has parameter values given by Figure 3.10. However, Filter #2 has an input impedance (Z_{OF2}) which is well apart from the output impedance of the EMI filter over all frequencies.

It is also seen from Figure 4.11 that the difference between phases of Z_{ID} and Z_{OF1} at frequencies of overlap is approximately 163 degrees. A load transient shown in Figure 4.3 is applied to the system shown in Figure 4.9, and the resultant output voltage of the source subsystem is shown in Figure 4.12. It can be seen that
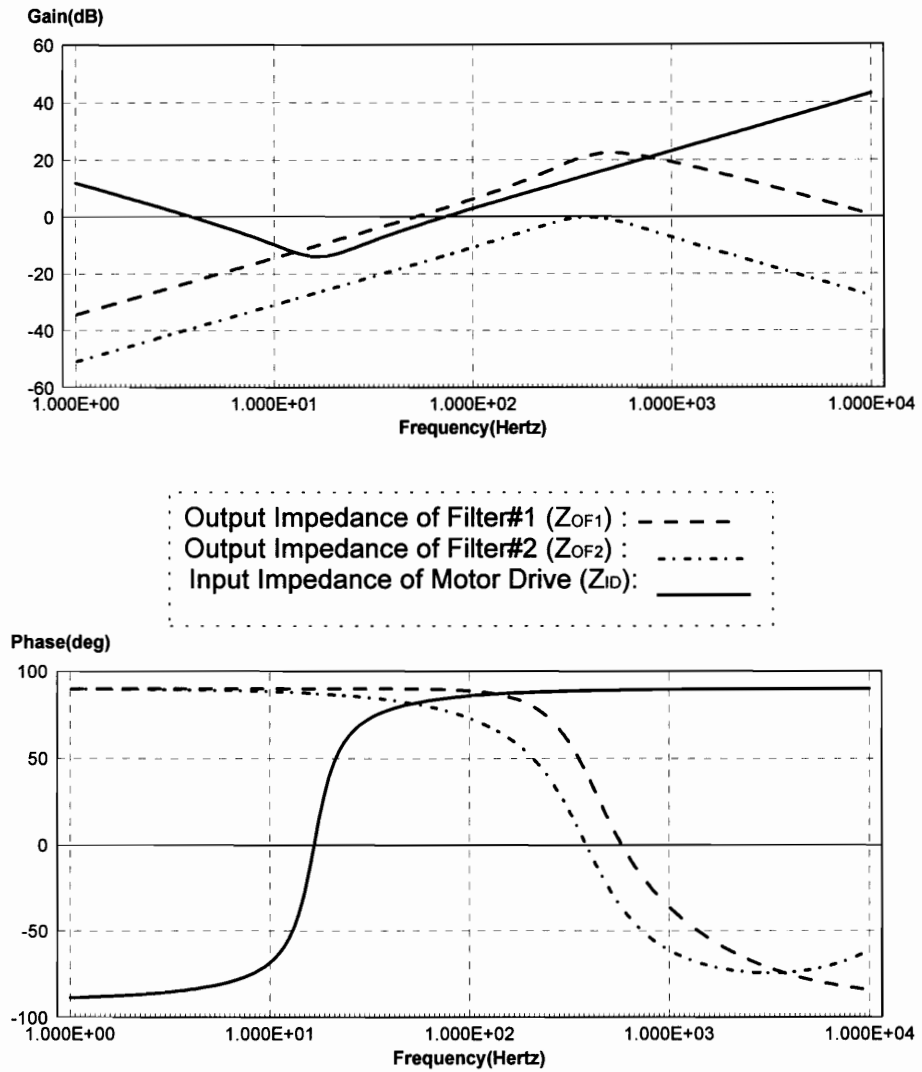
Figure 4.11 Comparison of Input Impedance of Inverter-fed PMSM Drive System (Z_{ID}) and Output Impedance of EMI Filter (Z_{OF})
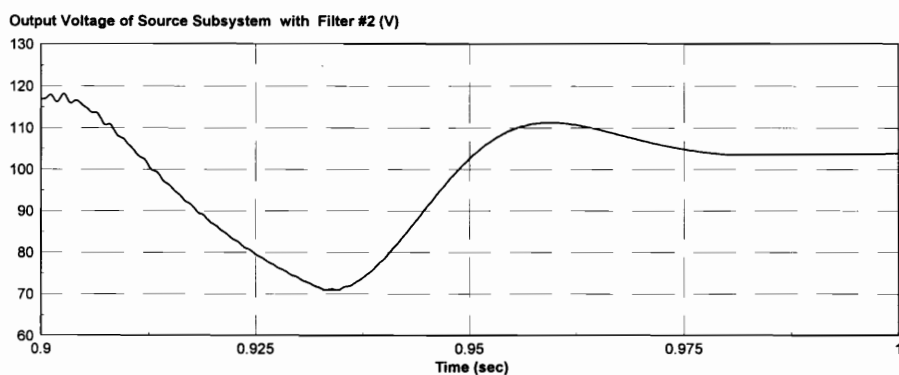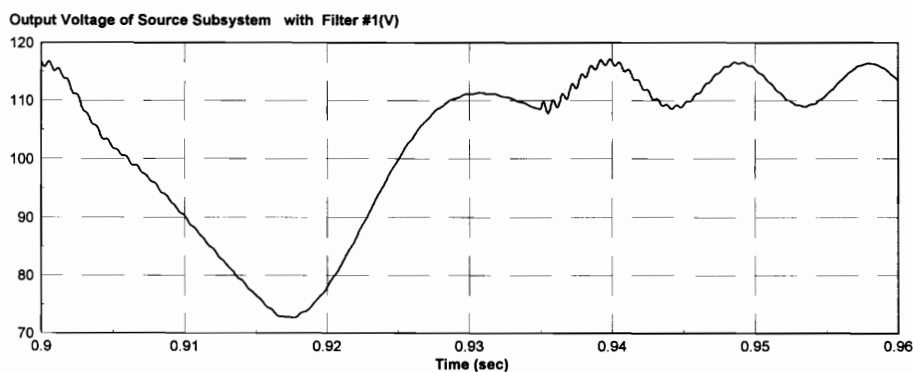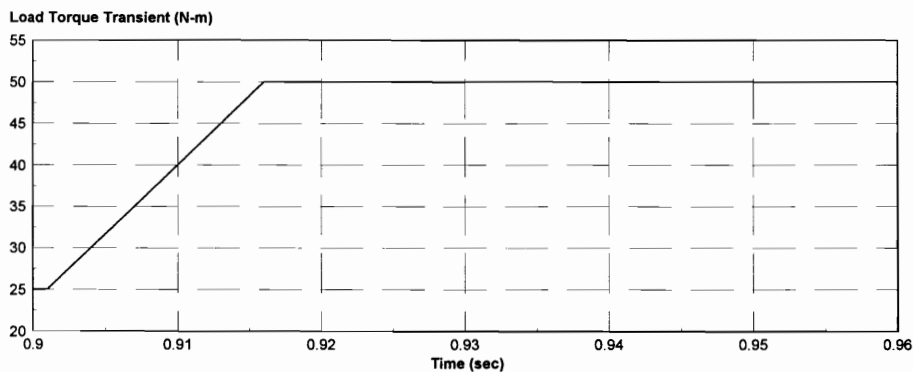
Figure 4.12 Transient Response of the Integrated System (DPS) Formed by Connecting the Load Subsystem using Filter #1 and Filter #2 in Section 4.4.1 to the Source Subsystem

the system formed with Filter #1 results in sustained oscillations in the output voltage of the source subsystem, while the system formed with Filter #2 has a stable response.

The conclusion from the above example can be summarized as:

The output impedance of the EMI filter when compared with the input impedance of the inverter-fed motor drive system should satisfy Criterion 2.1 (page 21).

It should also be noted that it is easier to satisfy the above condition if the frequencies of electromechanical resonance of the inverter-fed PMSM and the LC resonance frequency of the EMI filter are well separated. It was seen in Chapter 3 that for typical PMSM designs the electromechanical resonance frequency is in the range of few tens of Hz. In typical VSI designs the switching frequency is a few tens of kHz [17]. For this switching frequency, typical designs of EMI filter as shown in Appendix B, yield a corner frequency above several hundreds of Hz. This separation makes it easier to meet the above condition.

4.4.2 Interaction between the EMI Filter and the Source Subsystem

In the previous section (Section 4.4.1) the interaction between the EMI filter and the inverter-fed motor drive was studied, using output impedance of the EMI filter (Z_{OF}) and input impedance of the inverter-fed motor drive (Z_{ID}). In this section, the interaction between the EMI filter and the DC-DC converter is studied. In order to ensure minimal interaction between the DC-DC converter and

the EMI filter, the output impedance of the source subsystem ($|Z_{OS}|$) and the input impedance of the load subsystem ($|Z_{IL}|$) should not intersect; or if they do, the difference between the phases of Z_{OS} and Z_{IL} should not be close to 180 degrees. It was shown in Section 3.3.3 that $|Z_{IL}|$ is determined by the input impedance of the inverter-fed motor drive as well as the input impedance of the EMI filter. However, following the guidelines in Section 4.2, the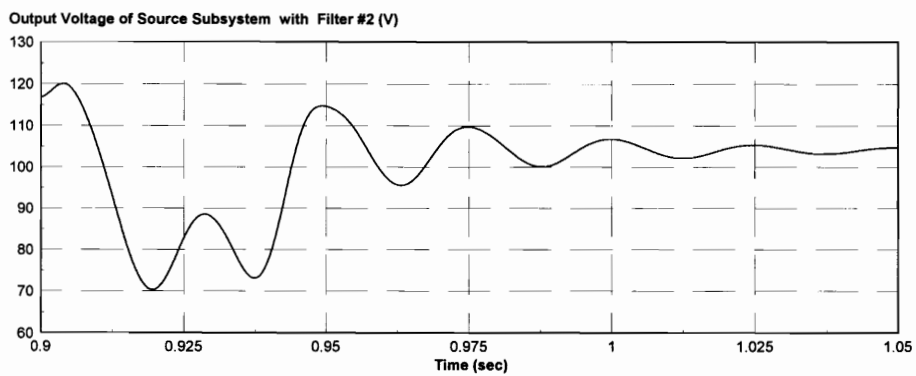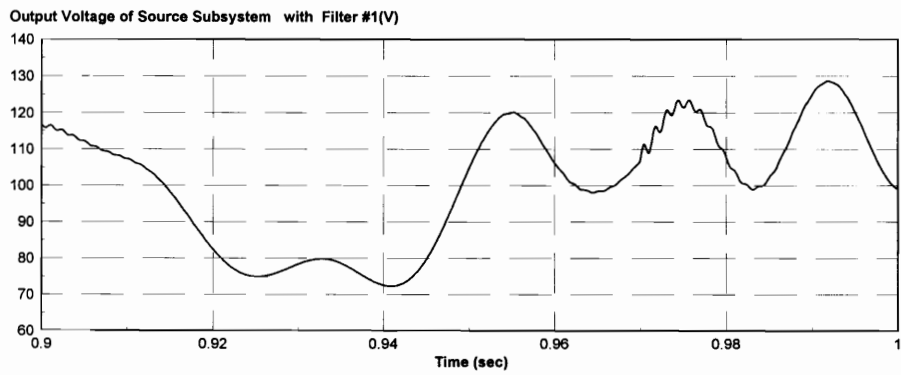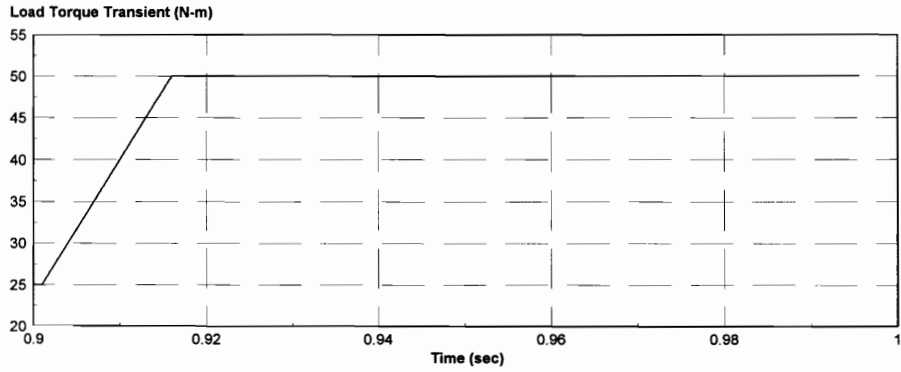 intersection between the that part of the input impedance of the load subsystem (Z_{IL}) which is due to the inverter-fed motor drive (electromechanical resonance at low frequencies) and the output impedance of the source subsystem (Z_{OS}) can be avoided. Hence, the important point to be considered now, is to avoid the intersection between that part of the input impedance of the load subsystem (Z_{IL}) which is due to the EMI filter (LC resonance at higher frequencies) and the output impedance of the source subsystem (Z_{OS}). Figure 4.13 shows the input impedance of the load subsystem (Z_{IL}) with two example filter designs, Filter #1 and Filter #2, compared with the output impedance (Z_{OS}). Both the filters are designed to give the required current attenuation as discussed in Appendix B. Since there is only one design constraint (desired attenuation) and multiple design parameters (L_1, L_2, R_1, C_1, and C_2) the constraint can be satisfied with different sets of component values. The parameter values of these two filters are:

Filter #1: $L_1 = 22$ μ H; $L_2 = 5$ μ H; $R_1 = 0.1$; $C_1 = 540$ μ F; $C_2 = 100$ μ F.

Filter #2: $L_1 = 220$ μ H; $L_2 = 5$ μ H; $R_1 = 1$; $C_1 = 54$ μ F; $C_2 = 100$ μ F.
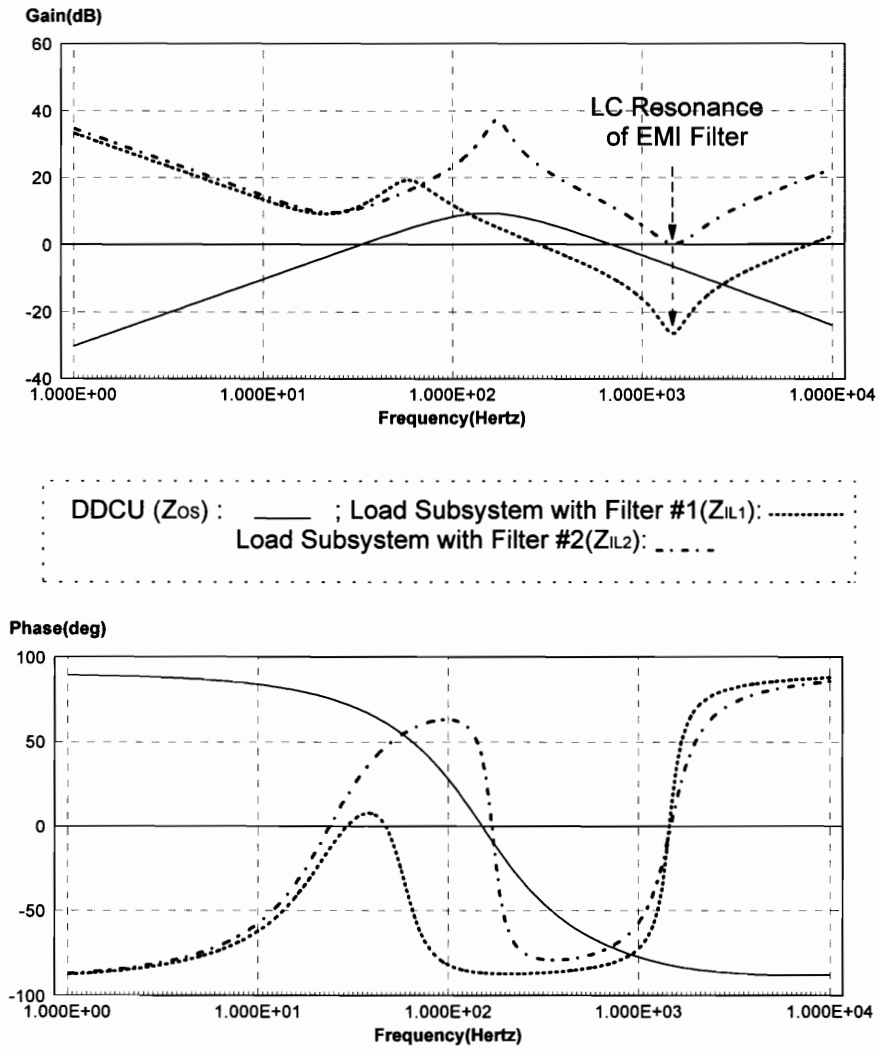
Figure 4.13 Output Impedance (Z_{OS}) of the Source Subsystem
Compared to Input Impedances (Z_{IL1}, Z_{IL2}) of Load Subsystems
formed with Filter #1 and Filter #2 given in Section 4.4.2

Load Torque Transient (N-m)

Output Voltage of Source Subsystem with Filter #1(V)

Output Voltage of Source Subsystem with Filter #2 (V)

**Figure 4.14 Transient Response of the Integrated System (DPS)
Formed by Connecting the Load Subsystem using Filter #1 and
Filter #2 in Section 4.4.2 to the Source Subsystem**

74

The PMSM used in both these cases is Motor #2 with the parameter values given by Figure 4.3. In case of load subsystem with Filter #1, that part of the input impedance of the load subsystem ($|Z_{IL}|$) which is due to the EMI filter (LC resonance) intersects with the output impedance of the source subsystem ($|Z_{OS}|$). The difference between the phases of Z_{OS} and Z_{IL} at frequencies of overlap is 166 degrees. This means a small-signal phase margin of 14 degrees for the DPS. The output voltage of the source subsystem when this DPS is subjected to large-signal disturbance in load torque shown in Figure 4.4, is shown in Figure 4.14. It can be seen that the system becomes unstable. However the system formed with Filter #2, has a stable transient response as shown in Figure 4.14.

The conclusion from the above examples can be summarized as:

The input impedance of the EMI filter when compared with the output impedance of the source subsystem should satisfy Criterion 2.1 (page 21).

Summarizing Sections 4.4.1 and 4.4.2 it can be said that *the L's and C's of the EMI filter should be so selected that in addition to satisfying the attenuation requirement of the EMI filter as described in Appendix B, i) The output impedance of the EMI filter when compared with the input impedance of the inverter-fed motor drive system should satisfy Criterion 2.1 (page 21).*
and ii) The input impedance of the EMI filter when compared with the output impedance of the source subsystem should satisfy Criterion 2.1 (page 21).

4.5 Summary

In this chapter, the stability issues that arise in a distributed power system (DPS) that uses an inverter-fed PMSM drive as a load subsystem were analyzed. The unique problems arising due to the unique input impedance characteristics of the inverter-fed motor drive operating without speed regulation were addressed. A series of examples showing that this unique nature can lead to performance degradation and instability in the DPS were presented. Using these examples as basis, design guidelines were developed to help in ensuring minimal interaction between the load subsystem made of inverter-fed motor drive, and the source subsystem. The guidelines were developed for motor, inverter as well as EMI filter design.

CHAPTER 5

CONCLUSIONS

The inverter-fed motor drive used as a load subsystem in a DPS was modeled in this thesis, and the input impedance characteristics of this load subsystem were analyzed in detail. The existence of unique features in the input impedance of the inverter-fed PMSM drive were shown. The interaction problems that these unique characteristics lead to were analyzed and a series of examples were presented. Design guidelines to alleviate these interactions were developed and presented.

Chapter 2 of this thesis highlighted the interaction issues arising while integrating a DPS. It was shown that in ensuring minimal interaction between the subsystems of a DPS after integration, the impedances of the subsystems were important design and analysis parameters. The effect of impedance overlap on the DPS performance was examined.

Chapter 3 of the thesis presented modeling and study of the input impedance of a typical inverter-fed motor drive system using a voltage source inverter and a permanent magnet synchronous motor. Two common operating modes of the drive system namely, operation without speed regulation and operation with speed regulation were studied. The existence of unique input impedance characteristics in the case of an inverter-fed motor drive system operating without speed regulation was shown. Analytical expressions as well as computer simulations were performed to study the input impedance. The unique input impedance characteristics were shown to be due to electromechanical resonance of the motor.

Chapter 4 analyzed the interaction problems that arise in the DPS due to the unique input impedance characteristics of the inverter-fed motor drive system. A series of examples were shown to demonstrate the unique interaction problems due to the motor-drive load subsystem. Design guidelines to ensure minimal interaction between the subsystems of a DPS using inverter-fed motor drive as a load subsystem were developed and presented.

The inverter-fed motor drive used as a load subsystem in a DPS was modeled in this thesis, and the input impedance characteristics of this load subsystem were analyzed in detail. The existence of unique features in the input impedance of the inverter-fed PMSM drive were shown. The interaction problems and performance degradation that these features can cause in the DPS were studied using a series of examples. Design guidelines to alleviate these interactions were developed and

presented. The use of these guidelines in designing an inverter-fed motor drive for use in a distributed power system application will help in minimizing the interaction problems that may arise due to the unique input impedance characteristics of the motor-drive load, and will ensure minimal performance degradation of the DPS.

APPENDIX A

Modeling of Three-phase Induction Motor

This appendix explains the modeling of three-phase induction motor. In Section 3.2.1 the three-phase permanent magnet synchronous motor was modeled in d-q co-ordinates and the equivalent electric circuit model was obtained. the input impedance was studied using that model. The three-phase induction motor can be similarly modeled.

The induction motor is different from the permanent magnet synchronous motor in that the induction motor has a rotor winding in place of the permanent magnet [19]. Hence the induction motor has additional dynamics due to the rotor winding.

The stator voltage equations of the induction motor in d-q co-ordinates (in stator reference frame) are given by [8]:

$$\sigma \, T_s \, \frac{di_d}{dt} + i_d = \frac{v_d}{R_s} - (1-\sigma)T_s \, \frac{di_m}{dt} + \sigma \, T_s \, w_1 \, i_q$$

$$(A.1)$$

$$\sigma \, T_s \, \frac{di_q}{dt} + i_q = \frac{v_q}{R_s} - (1-\sigma)T_s \, w_1 \, i_m - \sigma \, T_s \, w_1 \, i_d$$

$$(A.2)$$

The rotor voltage equation is [8]:

$$T_r \, \frac{di_m}{dt} + i_m = i_d$$

$$(A.3)$$

The electromechanical dynamics is given by [8]:

$$J \, \frac{dw}{dt} = k \, i_m \, i_q - w \, D - T_L$$

$$(A.4)$$

Rearranging these equations gives:

$$\sigma \, L_s \, \frac{di_d}{dt} + R_s \, i_d = v_d - (1-\sigma) \, L_s \, \frac{di_m}{dt} + \sigma \, L_s \, w_1 \, i_q$$

$$(A.5)$$

$$\sigma \, L_s \, \frac{di_q}{dt} + R_s \, i_q = v_q - (1-\sigma) \, L_s \, w_1 \, i_m - \sigma \, L_s \, w_1 \, i_d$$

$$(A.6)$$

$$L_r \, \frac{di_m}{dt} = (i_d - i_m) \, R_r$$

$$J \frac{dw}{dt} = k\, i_m\, i_q - w\, D - T_L$$

(A.8)

Equations (A.5)-(A.8) represent the model of the three-phase induction motor in d-q co-ordinates. In these equations:

$$w_1 = w + \frac{i_q R_r}{L_r i_m}$$

(A.9)

Also in the equations (A.1)-(A.9):

T_s , T_r - stator and rotor time constants respectively.

L_s , L_r - stator and rotor inductances (H) respectively.

R_s , R_r - stator and rotor resistances (Ω) respectively.

v_d, v_q - d, q axis stator voltages (V) of induction motor respectively.

i_d, i_q - d, q axis stator currents (A) of induction motor respectively.

σ - stator to rotor total leakage factor.

w - mechanical speed of the rotor (rad/sec).

J - Moment of inertia (Kg-m^2).

D - Damping co-efficient of the rotor (N-m/rad/sec).

T_L - Load Torque (N-m).

k - Electric Torque constant.

Equations (A.5)-(A.9) represent the large signal model of the induction motor and can be represented by the equivalent electric circuit form shown in Figure A.1. In this diagram there are four subcircuits. The two subcircuits on the left represent the q- and d- axis electrical part of the induction motor. The subcircuit at top on the right represents the electromechanical part of the induction motor. These three subcircuits are similar to those of the PMSM. However, the induction motor has an additional rotor winding and additional dynamics due to that winding. The subcircuit on the bottom right of Figure A.1 represents these dynamics.

By following a similar procedure as given in Section 3.2 for PMSM, the input impedance of the induction motor can be simulated using computer model. Using the results a similar procedure of impedance analysis can be performed.
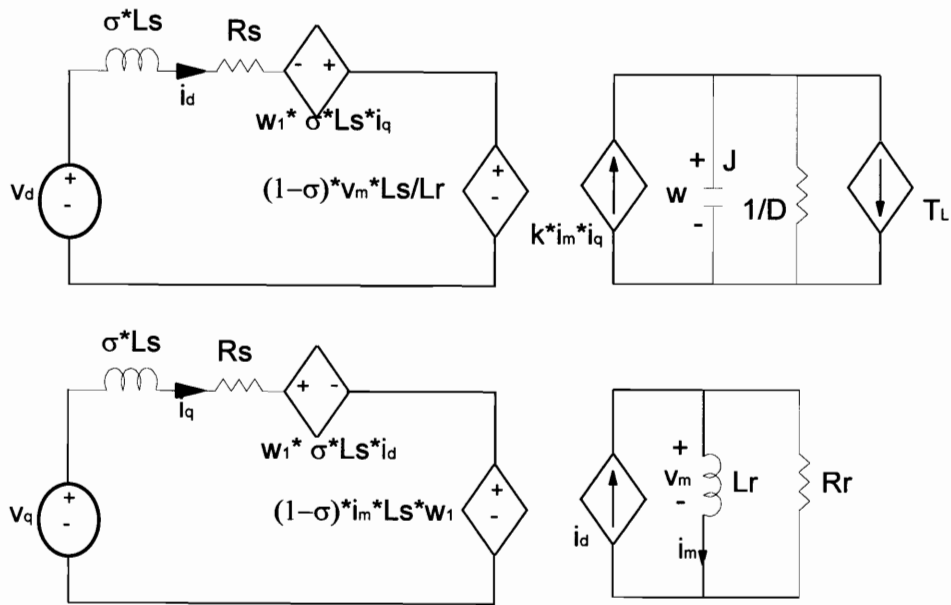
Figure A.1 Large-signal Average Model of Three-phase Induction Motor in d-q co-ordinates

APPENDIX B

Design of EMI Filter for VSI-fed PMSM Drive

This appendix explains an example design of the EMI filter for a voltage source inverter (VSI) fed PMSM drive.

Mechanical output power of PMSM in Figure 3.10 = P_{mech} = 3kW

Assuming efficiency of the PMSM = $\eta_{PMSM} = 0.8$ [17], yields:

Output Power of VSI = $P_o = \dfrac{P_{mech}}{\eta_{PMSM}} = 3.75$ kW

Assuming, efficiency of VSI = $\eta_{VSI} = 0.85$ yields:

Input Power of VSI = $P_{in} = \dfrac{P_o}{\eta_{VSI}} = 4.41$ kW.

DC input Voltage = V_{dc} = 120 V.

The average input DC current = $\dfrac{P_{in}}{V_{dc}}$ = 36 A.

Using the large signal model shown in Figure 3.3 it can be easily found that the ripple in the input current to the voltage source inverter for the motor described in Figure 3.10 is : I_{ripple} = 8A.

This ripple appears at switching frequency which is assumed to be 20kHz. Using the NASA standard on EMI requirements [20] : The maximum allowable ripple current for this inverter-fed PMSM drive at the frequency of 20kHz is: 0.05 A.

Hence the necessary attenuation at 20 kHz is: $20 * \log \dfrac{0.05}{8}$ = -58 dB.

Now the EMI filter should be designed to meet this attenuation. The topology shown in Figure 3.2 is used as the EMI filter. It is a good design practice to make $C_1 > C_2$ and $L_1 > L_2$ [18]. This helps in separating the low frequency and high frequency behavior of the filter. The filter should be designed such that the EMI attenuation requirements are met at the desired frequency of 20kHz. In order to reduce the size of the filter the first complex pair of poles due to resonance between C_1 and L_1 are designed to be around 1kHz. The following values of L_1 and C_1 are one pair of values to achieve this design.

$$L_1 = 21 \ \mu H.$$

$$C_1 = 540 \ \mu F.$$

R_1 should be designed so as to achieve the desired Q-factor for the filter. Designing for a Q=1 yields R_1=0.2 Ω. Now L_2 and C_2 are chosen so that the attenuation of the EMI filter at 20kHz is -58dB. The corresponding values of L_2 and C_2 are:

$$L_2 = 5 \ \mu H.$$

$$C_2 = 100 \ \mu F.$$

Thus this design of the EMI filter satisfies the EMI requirements of the standard [20].

REFERENCES

[1] S.E. Schulz, "System Interactions and Design Considerations for Distributed Power Systems," Master's Thesis, VPI&SU, Blacksburg, VA, January 1991.

[2] B.H. Cho, " Modeling and Analysis of Spacecraft Power Systems," Ph.D. Dissertation, VPI&SU, Blacksburg, VA, October 1985.

[3] L.R. Lewis, B.H. Cho, F.C. Lee, "Modeling, Analysis and Design of Distributed Power Systems," IEEE PESC, 1989, pp. 152-159.

[4] J. Liu, S. Schulz, B.H. Cho, F.C. Lee, "Design considerations for Distributed Power Systems," VPEC Seminar, Blacksburg, Virginia, 1989.

[5] C.M. Wildrick, "Stability of Distributed Power Supply Systems," Master's Thesis, VPI&SU, Blacksburg, VA, February 1993.

[6] L.R. Lewis, "Small-signal analysis and design of a distributed power system," Master's Thesis, VPI&SU, Blacksburg, VA, February 1990.

[7] S. Schulz, B.H. Cho, F.C. Lee, "Design considerations for a distributed power system," IEEE PESC, 1990, pp. 611-617.

[8] W. Leonhard, *Control of Electrical Drives*, New York: Springer-Verlag, 1984.

[9] P. Pillay, R. Krishnan, "Modeling, Simulation, and Analysis of Permanent-Magnet Motor Drives, Part I: The Permanent Magnet Synchronous Motor Drive," IEEE Transactions on Industry Applications, March/April 1989, pp. 265-273.

[10] S. Hiti, D. Borojevic, "Control of Front-End Three-Phase Boost Rectifier," APEC 1994, pp. 927-933.

[11] P.Huynh, "Stability Analysis of Large Scale Power Electronics Systems," PhD Dissertation, VPI&SU, Blacksburg, VA, Dec. 1994.

[12] B.H. Cho, J.R. Lee, "Design, Analysis and Simulation of the Main Bus Dynamics of Spacecraft Power Systems," IECEC 1995, pp. 547-553.

[13] R.Krishnan, A.J. Beutler, "Performance and design of an axial field permanent magnet synchronous motor servo drive, " Proceedings of IEEE IAS Annual Meeting, 1985, pp. 634-640.

[14] S. Hiti, D. Borojevic, "Small-signal Modeling and Control of Three-phase PWM Converters, VPEC Annual Seminar, 1994.

[15] Boeing Computer Services, "EASY5x Users Guide- EASY5 Engineering Analysis System, " 1992.

[16] Inland Motor, "Brushless DC Motors and Servo Amplifiers- Revision I, " 1990, Radford, VA.

[17] B.K. Bose, *Power Electronics and AC Drives*, New Jersey: Prentice-Hall, 1986.

[18] L. Huber, D. Sable, and F.C. Lee "Design of a High Efficiency DC-DC Converter for Electric Vehicle Auxiliary Battery Charger," VPEC Annual Seminar, 1994.

[19] A.E. Fitzgerald, C. Kingsley, and S.D. Umans, *Electric Machinery*, McGraw-Hill, New York, 1983.

[20] NASA, *Space Station Electromagnetic Emission and Susceptibility Requirements for Electromagnetic Compatibility*, Space Station Freedom Program Office, Revision A, Sept. 1991.

Vita

Musiri Shanmuga Paramasivam Shrivathsan was born in Salem, India on June 22, 1972. He received the B.S. degree in electrical engineering, with a Gold medal for academic excellence, from College of Engineering, Anna University, India in May 1993. In August 1993, he joined the Virginia Power Electronics Center at Virginia Polytechnic Institute and State University to begin research for the M.S. degree in Electrical Engineering, which he completed in July 1995. During his Master's he was selected as a member of the Honor Society of Phi Kappa Phi for his outstanding academic performance. After graduation, he will work for National Semiconductor Corporation in Santa Clara, California.